AD-A111 173 AIR FORCE INST OF TECH WRIGHT-PATTERSON AFB OH SCHOO--ETC F/G 20/6
DEVELOPEMENT OF A BACKWARD STIMULATED RAMAN SCATTERING SYSTEM F--ETC(U)
DEC 81 W D LINDSAY
UNCLASSIFIED AFIT/GEO/PH/81D-3 NL

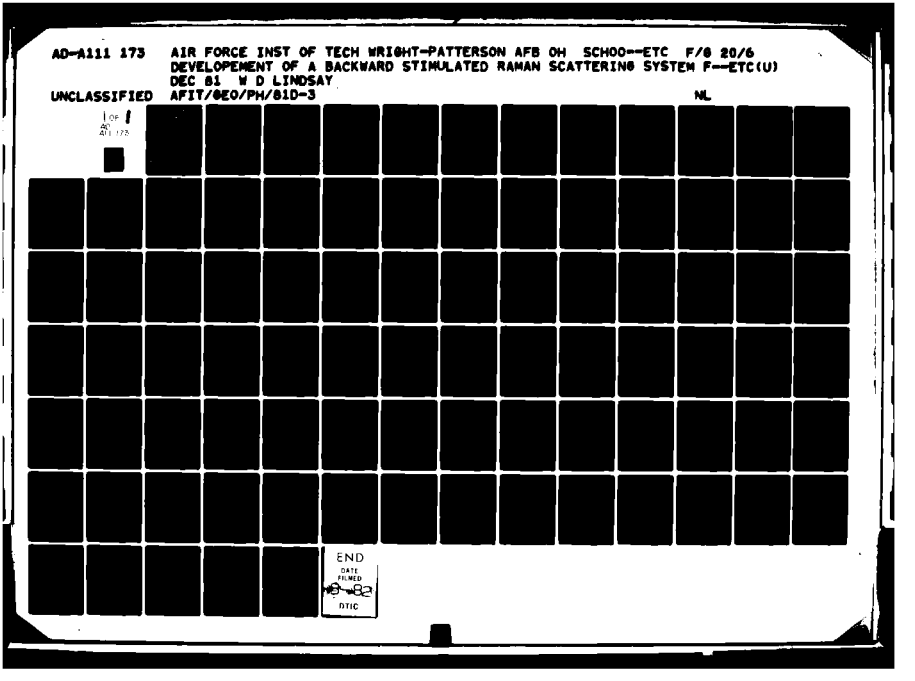

LEVEL II

AD A111173

DTIC
ELECTE
FEB 19 1982
S D
E

DTIC FILE COPY

DEPARTMENT OF THE AIR FORCE

AIR UNIVERSITY (ATC)

AIR FORCE INSTITUTE OF TECHNOLOGY

Wright-Patterson Air Force Base, Ohio

82 02 18 064

AFIT/GEO/PH/81D-3

LEVEL II

(1)

DEVELOPEMENT OF A BACKWARD STIMULATED RAMAN SCATTERING SYSTEM FOR PULSE COMPRESSION

THESIS

AFIT/GEO/PH/81D-3 William D. Lindsay
2nd Lt USAF

AFIT/GEO/PH/81D-3

DEVELOPEMENT OF A BACKWARD STIMULATED RAMAN SCATTERING SYSTEM FOR PULSE COMPRESSION

THESIS

Presented to the Faculty of the School of Engineering

of the Air Force Institute of Technology

Air University

in Partial Fulfillment of the

Requirements for the Degree of

Master of Science

by

William D. Lindsay, B.S.E.E.

2nd Lt USAF

Graduate Electro-Optics

December 1980

Preface

The purpose of this theses was to build an operational Raman pulse compression system and to determine the conditions under which the reverse Stokes output pulse was optimized. The output pulse was optimized for use in the measurement of semiconductor carrier diffusion processes by maximizing the output pulse energy while minimizing the pulsewidth. The test parameters for optimization were limited to the Raman cell gas pressure and the input pulse power. A theoretical model is also presented, which, although simplified, should provide a valuable reference for those interested in the backward stimulated Raman scattering process.

I owe a great deal of thanks to Paul Schreiber of the Aero Propulsion Laboratory for his helpful discussions on the theory of backward stimulated Raman scattering and to Dr. Won B. Roh of AFIT for his much needed assistance and guidance in his role as my advisor. Thanks also to Sig Kizirnis and Don Linder of the Aero Propulsion Laboratory and the University of Dayton, respectively, for their assistance in obtaining and building necessary equipment.

William D. Lindsay

Table of Contents

Table of Contents
(Continued)

List of Figures

List of Figures
(Continued)

Abstract

A Raman pulse compression system utilizing backward stimulated Raman scattering(BSRS) within a methane gas cell six feet in length was built and tested. A 12 MW giant pulse ruby laser with a pulsewidth of 12 ns(FWHM) was focused within the gas cell with a 10 cm focal length lens. The resulting reverse Stokes pulse at 8704 A had a maximum peak power of 15 MW and a minimum pulsewidth of 800 ps(FWHM). The peak power of the reverse Stokes pulse as well as the threshold power for BSRS were measured as a function of pressure. The shortest and most powerful reverse Stokes pulses were obtained in the pressure range of 150 - 175 psi with an input energy of 125 - 160 mJ. The short, intense pulses produced by this system should be useful in the investigation of events occuring on a subnanosecond time scale such as semiconductor carrier diffusion processes. The competing nonlinear processes of stimulated Brillouin scattering(SBS) and gas breakdown were also investigated and found to limit the efficiency of this system to 10 percent.

I Introduction

Backward stimulated Raman scattering (BSRS) has been used in several past experiments to concentrate the energy of a long laser pump pulse into a short reverse Stokes pulse. The resulting Stokes pulse may be as short as 100 piroseconds (ps) and is, therefore, useful in the investigation of events occurring on a subnanosecond time scale such as vibrational relaxation and semiconductor carrier diffusion processes. As the pump pulse energy is compressed into a much shorter reverse Stokes pulse, the resulting Stokes pulse intensity is much greater than the pump intensity. In this regard, the BSRS system functions like a Q-switch and can be used for high power systems where conventional Q-switching methods cannot be used. Also, the Stokes pulse is shifted in frequency from the pump pulse by 10-3000 cm^{-1}, and thus the BSRS system can be used to produce new laser frequencies. This paper will describe an experiment in which the optimal operating parameters are determined for a BSRS system using methane (CH_4) as a Raman medium and a giant pulse ruby laser as the pump source.

Background and History

The BSRS system is comprised of a Raman cell containing a Raman active medium, pulse sources, and required optics (See Figure (2)). As shown in Figure (1), a short Stokes pulse meets a long pump pulse within the Raman cell

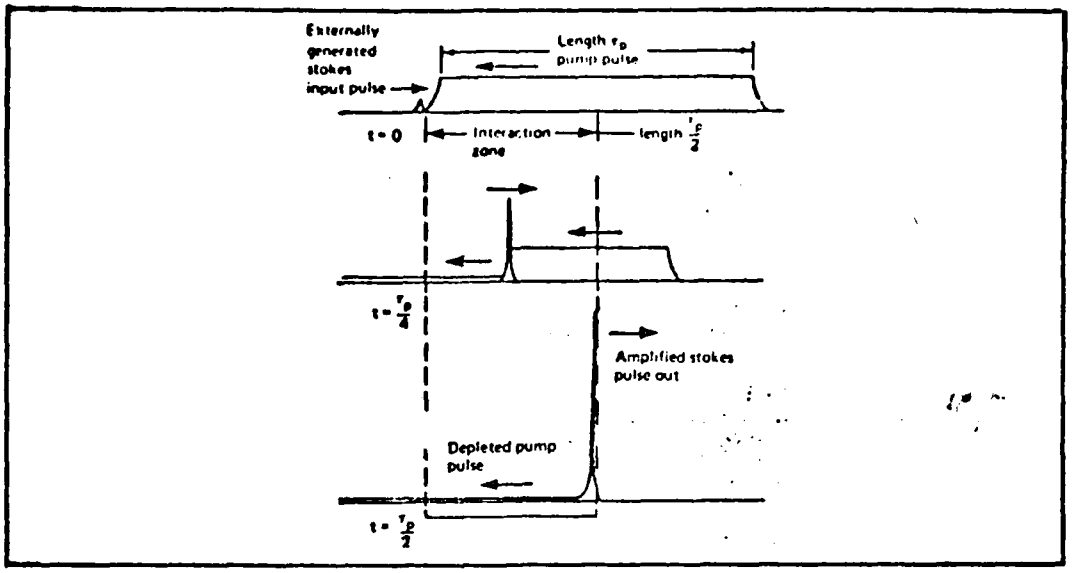

Fig. 1 Principle of Pulse Compression by Backward Raman Scattering (reprinted from Ref 15).

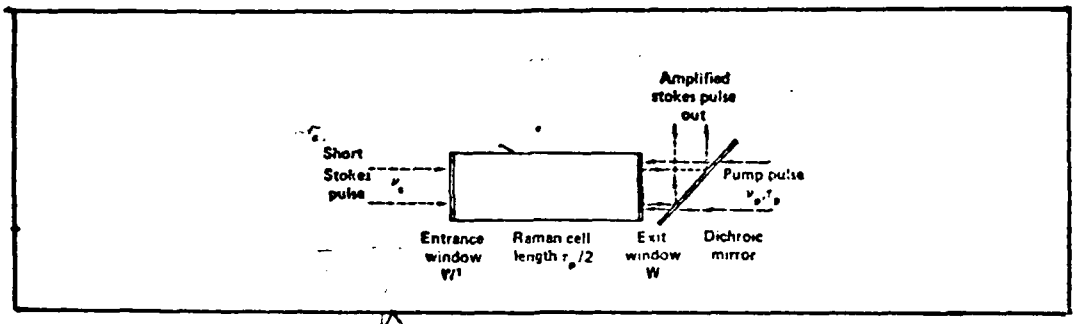

Fig. 2 Conceptual Layout of a Backward Raman Amplifier for Pulse Compression (reprinted from Ref 15).

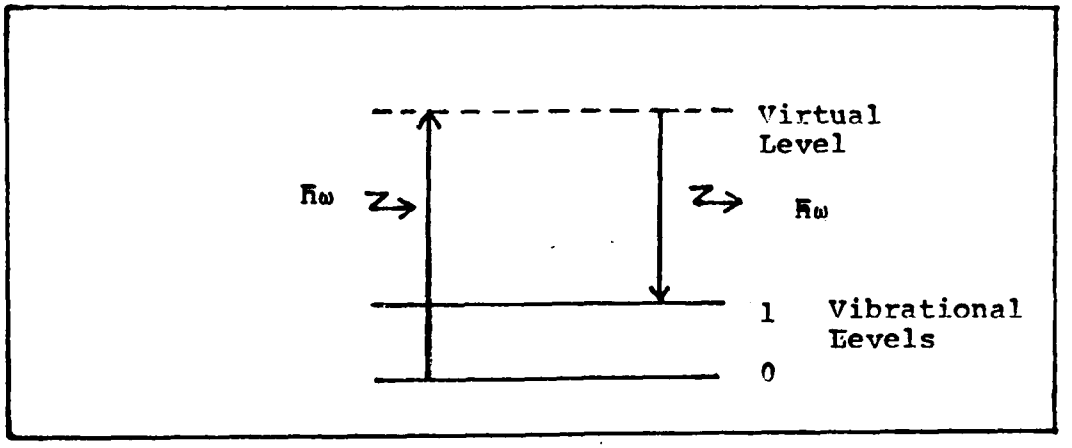

Fig. 3 Energy Level Diagram for Raman Scattering.

where a resonant energy transfer occurs in which pump energy at frequency ω_p is converted to Stokes energy as frequency ω_s. The frequency difference, $\omega_{01} = \omega_p - \omega_s$, corresponds to the vibrational frequency of the excited molecules in the Raman medium. Both the initiation and amplification of the Stokes pulse are stimulated Raman scattering (SRS) processes. The energy level diagram for SRS is shown in Figure (3). An input photon of energy $h\omega_p$ excites a molecule in the Raman medium to a virtual state which immediately reradiates another photon of energy $h\omega_s$. The energy difference is absorbed by the molecule. Since a virtual state is disallowed by quantum mechanics, a massive pumping intensity is required to achieve SRS. This intensity is normally achieved by focusing a giant pulse laser into the medium at the far end of the Raman cell. The high intensity at the focus creates an initial Stokes pulse in both the forward and backward directions. The forward pulse quickly exits the cell while the backward pulse travels through the pump pulse and extracts energy from it. The resulting Stokes pulse can be amplified by 30 times and compressed by 100 times compared to the pump pulse. In better controlled experiments, the uncertainty associated with the internal generation of the initial Stokes pulse is eliminated by using two Raman cells - one for generation and one for the amplification of the Stokes pulse. This method allows direct comparison to BSRS theory. Only one cell was available for this study and, hence, only a qualitative comparison with theory is permissable.

BSRS experimentation began after scientists observed short, intense light bursts resulting from the self-focusing of laser light in liquids. In 1966 Maier et al observed BSRS in a liquid CS_2 Raman cell pumped with a giant pulse ruby laser (Ref 9). They observed single Stokes pulses 30 ps wide with intensities 20 times that of the input pulse. They published a detailed theoretical paper along with further experimental data in 1969 (Ref 10). Brillouin scattering was said to prevent multiple Stokes pulses.

In 1968 Culver et al used a lens to focus a giant pulse ruby laser into an H_2 Raman cell. The resulting BSRS pulse was 300 ps wide and well controlled (Ref 2). They also noticed depletion of the pump pulse. Minck et al in 1967 observed both Raman and Brillouin scattering simultaneously under conditions of equal gain (Ref 12). This result was important in considering limitations to the Stokes intensity as discussed in Section II of this report. In 1974 Kachen focused 5324Å Nd Yag laser light into several gases and observed multiple forward and backward Raman pulses with widths of 100 ps. He found that the emitted pulses were Gaussian and that the pulses were shorter and more closely spaced for higher input power and shorter focal lengths. Murray et al, in 1978, studied the gain in a Raman medium by first creating a Stokes pulse by focusing a 248 nm KrF laser into a methane Raman cell and then injecting that Stokes pulse into a second Raman cell. This well-controlled experiment confirmed theoretical small signal gain values

for their system (Ref 13). A second experiment by this team found that the saturation fluence of their system was also correctly predicted by theory (Ref 14). In 1979 Murray et al published a detailed theoretical argument supporting the development of a large scale BSRS scheme for use in laser fusion (Ref 15). They predicted that an energy conversion of 50% is attainable with the Stokes output five times as intense and ten times shorter than the pump pulse. Further research by Perry et al in 1980 showed that a multiple pass Raman cell can be used to enhance efficiency (Ref 16).

The above-mentioned results were used in the development of the BSRS system for this experiment.

Problem and Scope

The objective of the research described in this paper was to design, build, and optimize a BSRS system capable of producing Stokes pulses with subnanosecond widths and megawatt intensities from a giant ruby laser pulse. Using previous reports as a guideline, the Raman cell length was made equal to one-half the pump pulse length (6 ft) and contained methane gas. The ruby light was focused into the Raman cell with an internal 10 cm focal length lens. Direct observation of Stokes pulses as well as competing processes were made as gas pressure and input power were varied. Since the initial Stokes pulse was internally generated, the intensity of the initial Stokes pulse was unknown and only qualitative comparison to BSRS theory was possible.

Threshold power levels for BSRS were measured as a function of pressure, an optimum operating range for pulse compression was determined, and an estimate of the small signal gain was made.

Approach

The giant pulse ruby laser was focused into the Raman cell to create the reverse Stokes pulse (and other undesired noise pulses). The pulses were selectively filtered and then detected with fast diodes and an R7912 transient digitizer of overall time constant of 750 ps. As the pressure and pump power were varied, the output pulses were monitored. Timing measurements were made by incorporating a reference pulse and path delay into the system.

Sequence of Presentation

The theory describing BSRS is discussed in Chapter II. The equipment and experimental procedure are described in Chapter III. Results and their analysis are presented in Chapter IV, the conclusions are presented in Chapter V, and ideas for future work are discussed in Chapter VI.

II Theory

The theory underlying the process of stimulated Raman scattering is well understood and has been verified in several past experiments (Ref 1-2). Raman scattering is a nonlinear process dependent on the third order nonlinear polarizability. The nonlinear polarizability can be derived either classically or semi-classically. The result can be used in Maxwell's equations to derive the radiation transfer equations which govern the transfer of energy from the pump pulse to the Stokes pulse. The semi-classical derivation of the nonlinear polarizability and the radiation transfer equations can be found in Appendix I. (The equations presented assume an injected Stokes pulse with no focusing.) This chapter is divided into two parts: (1) the solution of the radiation transfer equations, and (2) a description of the competing nonlinear processes which limit BSRS performance.

Radiation Transfer Equations

The radiation transfer equations can be written

$$-\frac{\partial I_s(x,t)}{\partial x} + \frac{n_s}{c}\frac{\partial I_s(x,t)}{\partial t} = \gamma I_s(x,t) I_p(x,t) \qquad (1)$$

$$\frac{\partial I_p(x,t)}{\partial x} + \frac{n_p}{c}\frac{\partial I_p(x,t)}{\partial t} = -\frac{\omega_p}{\omega_s}\gamma I_s(x,t) I_p(x,t) \qquad (2)$$

where I_s is the Stokes intensity, I_p is the pump intensity, n_s and n_p are the indices of refraction, ($n_s = n_p \simeq 1$ for

gas and so they are dropped), c is the speed of light, and γ is the Stokes gain coefficient given by

$$\gamma = \frac{4\pi^2 k_s (N_0 - N_1)}{\mu\, \omega_{01}\, \Gamma} \left(\frac{\partial\alpha}{\partial q}\right)^2 \frac{\Gamma^2}{(\omega_{01}-\omega)^2 + \Gamma^2} \tag{3}$$

where N_0 and N_1 are the population densities of the ground and excited states of the Raman medium, μ is the reduced mass, ω_{01} is the vibrational transition frequency, Γ is a damping constant equal to the Raman linewidth, $k_s = \omega_s/c$ is the Stokes wave vector, $\omega = \omega_p - \omega_s$ is the frequency difference between the pump and Stokes pulses, and $\partial\alpha/\partial q$ is the derivative of the polarizability with respect to internuclear separation.

The expression for γ may be simplified by assuming that the population inversion is small, $N_0 - N_1 \simeq N$, and that the system is at resonance, $\omega = \omega_{01}$. Further simplification is made by writing γ in terms of the measurable Raman scattering cross section, $\frac{\partial\sigma}{\partial\Omega}$, using

$$\left(\frac{\partial\sigma}{\partial\Omega}\right) = \left(\frac{2\mu\omega_0 c^4}{\hbar\, \omega^4}\right)\left(\frac{\partial\alpha}{\partial q}\right)^2 \tag{4}$$

where $\hbar = h/2\pi$ and h is plancks constant.

The resulting expression is

$$\gamma = \frac{8\pi^2 c^2 N}{h\omega_s^3 \Gamma} \left(\frac{\partial\sigma}{\partial\Omega}\right) \tag{5}$$

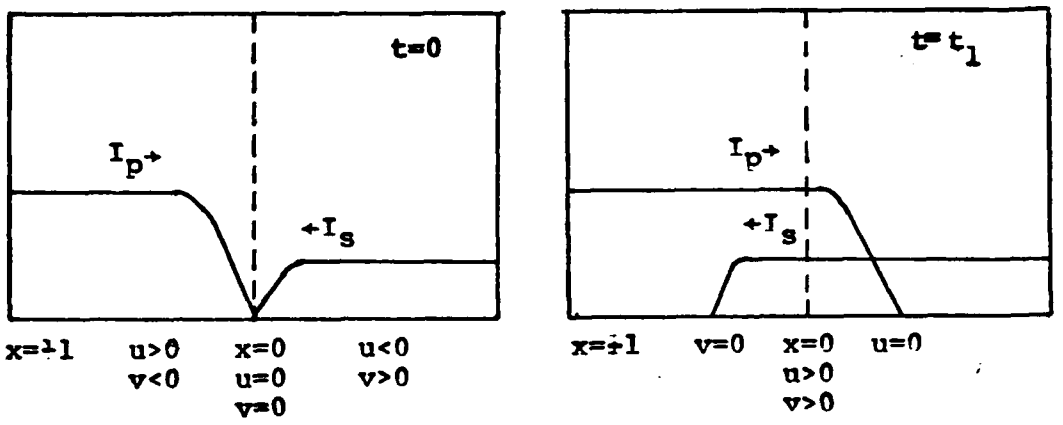

Fig. 4 Initial Conditions for BSRS Radiation Transfer Equations.

The solution to equations (1) and (2) is found in terms of the new variables u and v as shown in Figure (4):

$$u = t - x/c \tag{6}$$

$$v = t + x/c \tag{7}$$

u is a coordinate traveling with the pump pulse and v is a coordinate traveling with the Stokes pulse.

In terms of the new coordinates, equations (1) and (2) become

$$\frac{\partial I_s(u,v)}{\partial u} = \frac{2\gamma}{c} I_s(u,v) I_p(u,v) \tag{8}$$

$$\frac{\partial I_p(u,v)}{\partial v} = -\frac{2\gamma\omega_p}{c\omega_s} I_s(u,v) I_p(u,v) \tag{9}$$

For the case of small signal gain when $I_s << I_p$, constant pump intensity may be assumed, and the solution for the Stokes intensity is

$$I_s(u,v) = I_s(-\infty,v)\exp\left[\frac{2\gamma I_p u}{c}\right] \qquad (10)$$

The initial condition, $u=-\infty$, indicates that the pump pulse is far from the Stokes and thus $I_s(-\infty,v)$ is the initial Stokes pulse. The v coordinate is the position into the Stokes pulse. Exponential amplification of the Stokes pulse occurs as a function of the interaction depth u. Up to the point $u=0$, there is no interaction and no amplification. For $u>0$ the Stokes and pump pulse interact and amplification occurs. With I_p constant, no depletion of the pump is allowed, and hence the Stokes pulse retains its original shape.

Under realistic conditions, the pump pulse will be depleted and the gain seen by the interior of the Stokes pulse will be less than that seen on the leading edge. In this case the Stokes pulse is shortened and a more complex treatment is required. The following approach is adopted from a paper by Murray et al (Ref 15). Integration of equations (8) and (9) gives

$$I_p(u,v) = I_p(u,-\infty)\exp\left[-\frac{c\omega_p\gamma}{2\omega_s}\int_{-\infty}^{v} I_s(u,v')dv'\right] \qquad (11)$$

$$I_s(u,v) = I_s(-\infty,v)\exp\left[\frac{c\gamma}{2}\int_{-\infty}^{u} I_p(u',v)du'\right] \qquad (12)$$

Here $I_p(u,-\infty)$ is the initial pump pulse before interaction takes place.

A saturation fluence, S, is defined as

$$S = \frac{2\omega_s}{c\omega_p\gamma} \tag{13}$$

and energy fluences E_p and E_s are defined as

$$E_p(u,v) = \int_{-\infty}^{u} I_p(u',v)\,du' \tag{14}$$

$$E_s(u,v) = \int_{-\infty}^{v} I_s(u,v')\,dv' \tag{15}$$

The energy fluence for the Stokes pulse, E_s, is the energy per unit area up to point v in the Stokes pulse after interaction time u with the pump pulse. Likewise, E_p is the energy per unit area up to point u in the pump pulse after interaction time v with the Stokes pulse. If a single unit of area is assumed, the energy fluence can be described as the energy contained in the pulse up to a certain position in the pulse after a certain time during which energy has been transferred.

The above definitions yield the following when used in equations (11) and (12)

$$I_p(u,v) = I_p(u,-\infty)\exp\left[-\frac{E_s(u,v)}{S}\right] \tag{16}$$

$$I_s(u,v) = I_s(-\infty,v)\exp\left[\frac{\omega_s}{\omega_p}\frac{E_p(u,v)}{S}\right] \tag{17}$$

The pump intensity falls exponentially to 1/e of its initial value after the passage of the saturation fluence, S.

Similarly, the Stokes pulse grows exponentially in total fluence of the pump pulse. The leading edge of the Stokes pulse sees the constant gain of the undepleted pump pulse and is thus amplified more than the remainder of the pulse.

Equations (16) and (17) can be solved using several substitutions and integration techniques. (For clarity, the functional form of I_s and I_p will be omitted where possible.) Integration of equation (8) with respect to v yields

$$\int_{-\infty}^{v} \frac{\partial I_s}{\partial u}\, dv' = \frac{\omega_s}{\omega_p S} \int_{-\infty}^{v} I_s I_p dv \tag{18}$$

Differentiation of equation (15) with respect to u and v yields the relations

$$\frac{dE_s}{dv} = I_s(u,v) \tag{19}$$

$$\frac{\partial E_s}{\partial u} = \int_{-\infty}^{v} \frac{\partial I_s(u,v')}{\partial u}\, dv' \tag{20}$$

Equations (19), (20), and (16) may be used to write equation (18) in terms of the Stokes energy fluence, $E_s(u,v)$,

$$\frac{\partial E_s(u,v)}{\partial u} = \frac{\omega_s}{\omega_p S} I_p(u,-\infty) \int_{-\infty}^{E_s} \exp\left[-\frac{E_s(u,v)}{S}\right] dE_s \tag{21}$$

Evaluation of the integral in (21) leads to

$$\frac{\partial E_s(u,v)}{\partial u} = \frac{\omega_s}{\omega_p S} I_p(u,-\infty)\left(1 - \exp\left[-\frac{E_s(u,v)}{S}\right]\right) \tag{22}$$

This equation can be integrated by making the substitution

$$\phi_s(u,v) = \exp\left[\frac{E_s(u,v)}{S}\right] - 1 \qquad (23)$$

Equation (22) then becomes

$$\frac{\partial \phi_s(u,v)}{\partial u} = \frac{\omega_s I_p(u,-\infty)}{\omega_p S}\,\phi_s(u,v) \qquad (24)$$

which has for a solution

$$\phi_s(u,v) = \phi_s(-\infty,v)\exp\left[\frac{\omega_s}{\omega_p S}\int_{-\infty}^{u} I_p(u',-\infty)\,du'\right] \qquad (25)$$

which can be written using equation (14) as

$$\phi_s(u,v) = \phi_s(-\infty,v)\exp\left[\frac{\omega_s}{\omega_p}\,\frac{E_p(u,-\infty)}{S}\right] \qquad (26)$$

Equation (26) expresses the Stokes saturation function, $\phi_s(u,v)$, in terms of the known quantities, $\phi_s(-\infty,v)$ and $E_p(u,-\infty)$. $\phi_s(-\infty,v)$ is the initial Stokes saturation defined in equation ( ) and dependent only on $E_s(-\infty,v)$. The Stokes energy fluence, $E_s(-\infty,v)$, is simply the integral of the initial Stokes intensity up to point v in the Stokes pulse. $E_p(u,-\infty)$ is similarly defined as the initial pump energy fluence which is also known. The significance of the function, $\phi_s(u,v)$, is seen in the following way:

$$\phi_s(u,v) = \frac{1 - \exp\{-E_s/S\}}{\exp\{-E_s/S\}} = \frac{I_p(u,-\infty) - I_p(u,v)}{I_p(u,v)} \quad (27)$$

From equations (26) and (27) it is clear that the ratio of depleted pump intensity to the pump intensity remaining grows exponentially with the pump fluence and depth of penetration, u, at a point v in the Stokes pulse. The exponential term in equation (26) is the small signal gain seen by the leading edge of the Stokes pulse. The small signal gain is written

$$G(u) = \frac{\omega_s}{\omega_p} \frac{E_p(u,-\infty)}{S} \quad (28)$$

At $v = -\infty$ in G(u) above the pump pulse has its original shape with respect to u, and the gain is at a maximum. In the original expression for I_s, equation (17), the gain was exponential in $E_p(u,v)$ and explicitly showed how gain was reduced as the pump pulse was depleted.

Equation (26) can be used to express the intensity in terms of known functions. Using equation (19) the Stokes intensity, $I_s(u,v)$, is

$$I_s(u,v) = I_s(-\infty,v) \frac{dE_s(u,v)}{dE_s(-\infty,v)} \quad (29)$$

Equation (23) can be written as

$$E_s(u,v) = S \ln[\phi_s(-\infty,v)e^{G(u)} + 1] \quad (30)$$

The resulting equation for the Stokes intensity is

$$I_s(u,v) = I_s(-\infty,v)\,\frac{e^{G(u)}\,[\phi_s(-\infty,v) + 1]}{e^{G(u)}\,\phi_s(-\infty,v) + 1} \qquad (31)$$

The pump intensity can be found using equations (16) and (30)

$$I_p(u,v) = I_p(u,-\infty)\,\frac{1}{e^{G(u)}\,\phi_s(-\infty,v) + 1} \qquad (32)$$

Again, in the limit of small signal gain and undepleted pump pulse when

$$\phi_s(-\infty,v)\,e^{G(u)} \ll 1 \qquad (33)$$

the equations become

$$I_s(u,v) = I_s(-\infty,v)\,e^{G(u)} \qquad (34)$$

$$I_p(u,v) = I_p(u,-\infty) \qquad (35)$$

This is always the case on the leading edge of the Stokes pulse where $v = 0$, and $\phi_s(u,v) \approx 0$.

Understanding of equations (31) and (32) can be enhanced by division and substitution for $\phi_s(-\infty,v)$ from equation (23). The result is

$$\frac{I_s(u,v)}{I_p(u,v)} = \frac{I_s(-\infty,v)}{I_p(u,-\infty)}\,\exp\left[\frac{\omega_s}{\omega_p}\,\frac{E_p(u,-\infty)}{S} + \frac{E_s(-\infty,v)}{S}\right] \qquad (36)$$

The ratio of Stokes to pump intensity at the point (u,v) grows exponentially with the small signal gain, G(u), plus the added factor, $E_s(-\infty,v)/S$, which accounts for the depletion of the pump pulse.

The final Stokes intensity after passage through the Raman cell is $I_s(-\infty,v)$

$$I_s(\infty,v) = I_s(-\infty,v)\,\frac{e^{G(\infty)}\left(\phi_s(-\infty,v) + 1\right)}{e^{G(\infty)}\phi_s(-\infty,v) + 1} \qquad (37)$$

Equation (37) shows that the final Stokes intensity is dependent only on the initial Stokes pulse and the initial total pump fluence. Implicitly assumed is that the pump pulse length is limited to twice the Raman cell length. Also, under the conditions of this experiment the pump pulse is responsible for producing the initial Stokes pulse. This point is not included in equation (37), but requires the pump pulse to exceed a certain threshold energy.

In the simple case of square Stokes and pump input pulses, the peak intensity for the Stokes pulse occurs on its leading edge where v = 0 and

$$I_s(\infty,0) = I_s(-\infty,0)e^{G(\infty)} \qquad (38)$$

The half width at half maximum, $\theta\frac{1}{2}$, is

$$\theta\frac{1}{2} = \frac{S}{I_s(-\infty,0)}\ln\left(\frac{e^{G(\infty)} - 1}{e^{G(\infty)} - 2}\right) \simeq \frac{Se^{-G(\infty)}}{I_s(-\infty,0)} \qquad (39)$$

where $G(\infty)$ is assumed large.

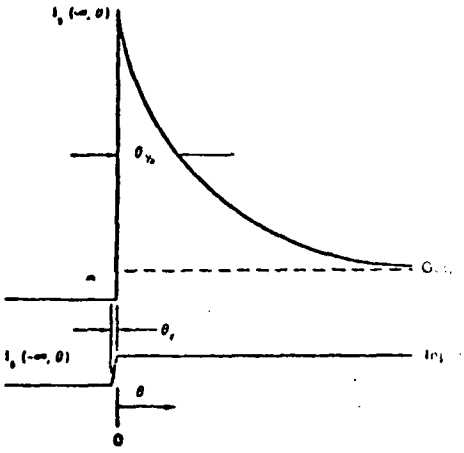

Fig. 5 Stokes Output for a Square Wave Stokes Input (reprinted from Ref 15).

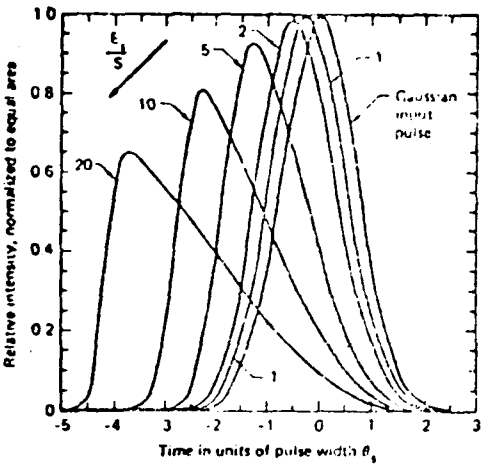

Fig. 6 Stokes output for a Gaussian Input as a Function of Energy Fluence at the Output. Pulse shapes are normalized to equal area (reprinted from Ref 20).

The Stokes output for a square pulse input is shown in Figure (5). This is an excellent illustration of how the initial pulse is shortened: the leading edge of the pulse sees maximum gain while the interior sees progressively less, hence a shortening effect is observed. The results for a Gaussian pulse are shown in Figure (6).

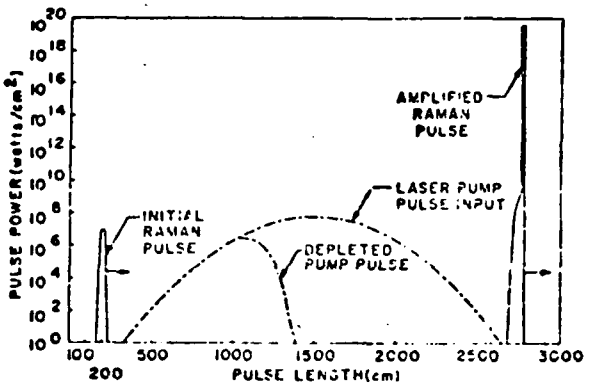

Fig. 7 Computer Plots of the Numerical Solution to the Radiation Transfer Equations (reprinted from Ref 2).

A computer plot of the solutions to the radiation transfer equations is shown in Figure (7) which shows the depletion of the pump pulse. The leading edge of the pump pulse is not depleted because of the finite time required for the buildup of gain, G(u). The amplification of the Stokes pulse causes a very narrow and intense spike to grow on the leading edge of the Stokes pulse, as expected.

The objective of this experiment is to obtain the narrowest and most intense Stokes output pulse. As seen from equations (38) and (39), this implies maximizing the gain, G(∞). From equations (28), (13) and (14) the gain can be written

$$G(\infty) = \frac{\omega_s}{\omega_p S} \int_{-\infty}^{\infty} I_p(u', -\infty)\, du'$$

$$= \frac{c\gamma}{2} \int_{-\infty}^{\infty} I_p(u', -\infty)\, du' \qquad (40)$$

where γ is defined in equation (5)

$$\gamma = \frac{8\pi^2 c^2 N}{h\omega_s^3 \Gamma} \left(\frac{\partial\sigma}{\partial\Omega}\right) \tag{5}$$

The damping constant Γ is defined as, $\Gamma = \pi\Delta\nu_R$, where $\Delta\nu_R$ is the Raman linewidth (FWHM). The line broadening due to pressure in methane is nearly cancelled by the collapse of the closely spaced rotational lines in the Q branch of methane. The linewidth is then nearly constant from 1-10 atm at $\Delta\nu_R = .3\ cm^{-1}$ (Ref 15). The Raman cross section, $\partial\sigma/\partial\Omega$, is also nearly constant in this range and given by $\partial\sigma/\partial\Omega = 1.9\text{x}10^{-29}\ cm^2/sr\text{-}mol$ (Ref 20). Thus the gain is dependent only on the pressure (number density, N) of the gas, and the total energy fluence of the pump pulse. With the Stokes frequency, $\omega_s = 2.165 \times 10^{15}$ rad/sec, γ is given by

$$\gamma = 9.76\text{x}10^{-12} \times p(atm)\ m/watt \tag{41}$$

Typical operating points for this experiment are

$$p = 10\ atm \tag{42}$$

and

$$\int_{-\infty}^{\infty} I_p(u',-\infty)du' = 1.91\text{x}10^3\ J/m^3 \tag{43}$$

for which

$$G(\infty) = 27.7 \tag{44}$$

The location of energy in the output pulse is another factor which requires consideration. Only the energy between the half power points is useful, the rest being lost in the tail of the pulse. Thus, the useful energy output is less than expected. Other limitations to the Stokes output are described in the next section.

Competition between Nonlinear Processes

The preceding theory assumed the existence of only two interacting waves, the reverse Stokes pulse and the laser pump pulse. The Rayleigh scattering, anti-Stokes scattering and secondary Stokes scattering were ignored because of their small intensities (See Appendix I). This was a very reasonable approximation, but other nonlinear effects also occur and should be mentioned. A forward traveling Stokes pulse and backward traveling Brillouin pulse are present, and a second Stokes pulse may be generated from the first. The mixing of the waves in a four wave parametric process may occur if phase conditions are met, but they are negligible for this experiment. Self focusing and multi-photon absorption are processes that occur only for intensity conditions much greater than those encountered in this experiment. Gas breakdown is another nonlinear process which could occur and may be important when the input pulse is focused. This section will discuss the important nonlinear processes mentioned above in more detail and describe their effect on the reverse Stokes pulse.

Forward Stokes Pulse. A forward Stokes pulse may be generated and amplified in the same way as the reverse Stokes pulse. The forward Stokes pulse, however, has access only to the volume of pump energy that it travels with, while the reverse Stokes pulse sweeps through the entire pump pulse. For the conditions of this experiment, where the input pump pulse is focused at the far end of the Raman cell, the forward pulse has almost no time to develop and be amplified. Other nonlinear pulses more intense than the original pump pulse may generate forward Stokes pulses, however. The gain for both forward and backward Stokes pulses is inversely proportional to the Raman linewidth, but this linewidth is generally less in the forward direction.

One contribution to the forward-backward gain difference is the asymmetry in the Doppler broadening of the Raman linewidth. The shift in the forward direction is $-(\nu_p-\nu_s)v/c$, and the shift in the backward direction is $-(\nu_p+\nu_s)v/c$, where ν_p is the pump frequency, ν_s is the Stokes frequency, v is the velocity of the scattering molecule, and c is the speed of light. The much larger shift in the backward direction means that the Doppler contribution to the Raman linewidth in the backward direction will be much greater than that in the forward direction (perhaps by a factor of 25). This effect is reduced at higher pressures where broadening effects independent of direction predominate (Ref 15).

Another contribution is the effect of pump linewidth. The forward Stokes pulse is generated from noise phonons which can couple with all frequencies in the pump pulse. In the case of the backward Stokes pulse, the phonons can only couple with the pump frequencies within the Raman linewidth, and so the forward gain is enhanced if the pump linewidth is greater than the Raman linewidth (Ref 15).

Intensity fluctuations in the pump pulse also favor forward gain. The backward Stokes gain is proportional to the average pump intensity, but the forward gain is proportional to the peak intensity. If the pump pulse has regions of high intensity, forward Stokes emission may take place in the Raman cell before the pump pulse is focused and a backward pulse is generated.

In this experiment, no effect from pump linewidth is expected since the laser linewidth (.034 cm^{-1}) is smaller than the Raman linewidth (.3 cm^{-1}). Also, since the pressure is fairly high at 10 atm, the Doppler asymmetry should also be small. The Gaussian pump pulse is smooth, but the reamplified Brillouin pulse (discussed below) reaches high intensities and could stimulate a forward Stokes pulse. Murray et al measured a forward-backward gain ratio for methane of about 2 using a 248 nm KrF laser source.

Backward Second Stokes Superfluorescence. The intensity of the first backward Stokes pulse may be great enough to stimulate a second Stokes pulse in the same direction

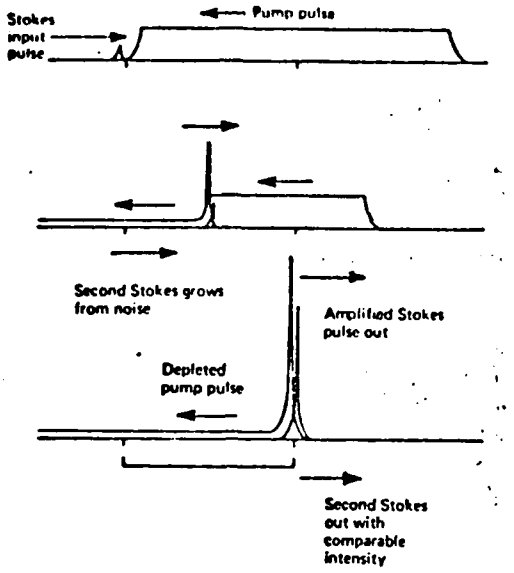

Fig. 8 Growth of Superfluorescent Backward Second Stokes. The backward first Stokes pulse serves as a pump producing gain at the second Stokes frequency (reprinted from Ref 15).

(See Figure (8)). The second Stokes pulse is shifted in frequency from the first by $-\omega_{01}$, the vibrational frequency of the Raman medium. A second Stokes pulse generated from a narrow band pump and first Stokes pulse will have the high divergence typical of superfluorescence and is of little use. In a typical Raman amplifier, a second Stokes gain of 20 is permissible; higher gains would cause depletion of the first Stokes pulse (Ref 15). Since the second Stokes pulse is from a forward scattering process, the reverse Stokes gain is limited by this process to about 10. Since the input pulse in this experiment is focused, initial second Stokes pulses may be generated at the focal point, and the permissible gain will be less.

Stimulated Brillouin Scattering (SBS). A further limit to the reverse Stokes emission is SBS. In SBS, incoming photons are scattered from acoustic phonons in the media, and hence the relaxation time is large and the frequency shift is small. A typical relaxation time for SBS is 1 ns (compared to 1 ps for BSRS), and a typical frequency shift is 1 cm^{-1} (compared to 1000 cm^{-1} for BSRS). In their simplest form, the governing radiation transfer equations for SBS are identical to those for BSRS except for the constants. Thus, one would expect the same sort of pulse compression from SBS. This pulse compression has been observed by Hon who has observed backward Brillouin pulses 2 ns wide in 130 atm of methane (Ref 5). Forward SBS can be observed only if the pump pulse is more than 20 ns long and is not expected in this experiment (Ref 7).

In most gases, only the nonlinear process with the highest gain is observed, but methane represents a special case in which both SBS and SRS occur. Figure (9) shows the experimentally determined gain for SBS and SRS as a function of pressure (Ref 12). The Raman gain saturates at about 20 atm due to pressure broadening of the Raman linewidth, and above this point the Brillouin gain continues to rise. Therefore, operation below 20 atm is desirable. Due to the much quicker relaxation time of BSRS, it begins before SBS gets started and starts to deplete the pump pulse before it can be scattered by SBS. Thus,

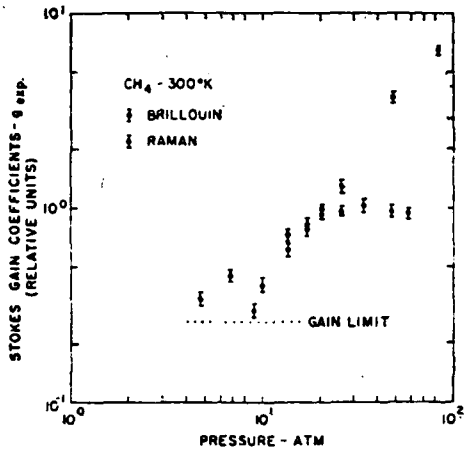

Fig. 9 Experimental Gain Coefficients for SBS and SRS in CH_4 at 300°K. The data points are calculated from threshold data (reprinted from Ref 12).

SBS should be only a small problem in this system. It should be noted that the Brillouin pulse may prevent multiple reverse Stokes pulses (Ref 10). Also, since the Brillouin light is essentially unshifted in frequency, it may reenter the laser system and be reamplified. This can be avoided by keeping a large separation between laser and gas cell, or using a polarizing plate and $\lambda/4$ wave plate. In this experiment the Brillouin pulse was allowed to reenter the laser, and the resulting reamplified pulse subsequently produced both forward and backward Raman pulses!

Gas Breakdown. The last competing process to be discussed is the ionization of the gas in the path of the laser light, gas breakdown. Gas breakdown occurs at laser intensities on the order of 10^{11} w/cm^2 and manifests itself in the form of a bright flash of white light and simultaneous absorption of laser energy. Intensities of this order

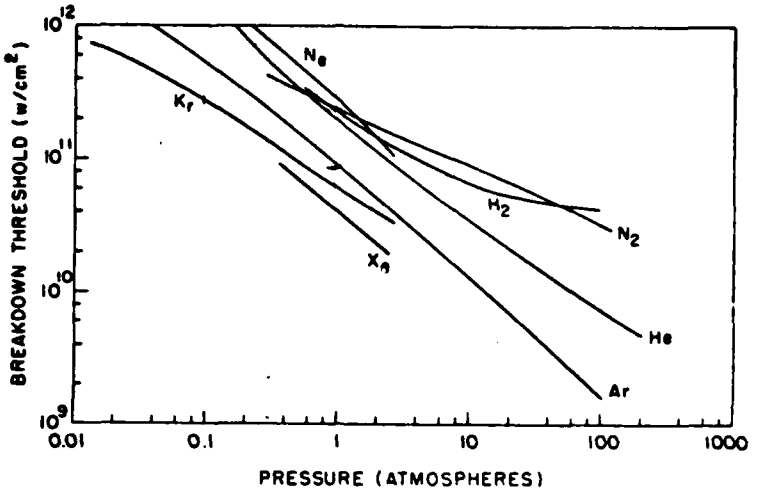

Fig. 10 Experimental Results of Breakdown Threshold vs. Pressure for Several Gases (reprinted from Ref 17).

occur only at the focal point of a Q-switched laser pulse. The temperature at the focal point during breakdown is often great enough to cause an audible shock wave due to the extremely rapid expansion of the gas. The high intensities are needed to overcome the threshold for which multiphoton absorption can produce free electrons in the focal region. The free electrons then absorb more energy from the laser light and transfer it via collisions to ionize further molecules in a cascade effect. Neither the initial nor the subsequent buildup of the breakdown process is well understood (Ref 17).

The threshold intensity and the time required for breakdown decreases as laser power, gas pressure, and focal volume increase. As laser intensity is increased the time

after the pulse edge at which breakdown occurs is decreased by as much as 30 ns/10^{10} w/cm^2. The effect of gas pressure is more pronounced as shown in Figure (10). The threshold for Argon, for example, decreases at a rate of 10^8 w/cm^2/ atm. Above 100 atm the threshold begins to increase due to the increased loss of free electrons from collisions outside the focal region. For the same reason, threshold for breakdown increases as the focal spot size decreases. This effect is offset by the corresponding decrease in intensity at the focal point (Ref 17).

The frequency dependence of the breakdown threshold is shown in Figure (11). Although this data is for Argon only, other gases have a similar frequency dependence. At low frequencies the threshold increases as predicted by classical microwave theory, but at high frequencies the photon energy becomes comparable to the ionization energy and this behavior is no longer followed (Ref 17).

Gas breakdown has been observed in 2 atm of methane at a frequency of 347 nm at 2×10^{10} w/cm^2 (Ref 15). Also, breakdown in 10 atm at a frequency of 248 nm was observed when an intensity of 5×10^6 w/cm^2 was focused by a 20 m focal length lens (Ref 13). In the later case, breakdown was avoided by switching to a 20 m focal length. The experiment to be discussed in this paper uses a 10 MW ruby laser with a divergence $\theta \simeq 1$ mrad. The beam is focused by a lens with focal length f = 10 cm. The spot size d is

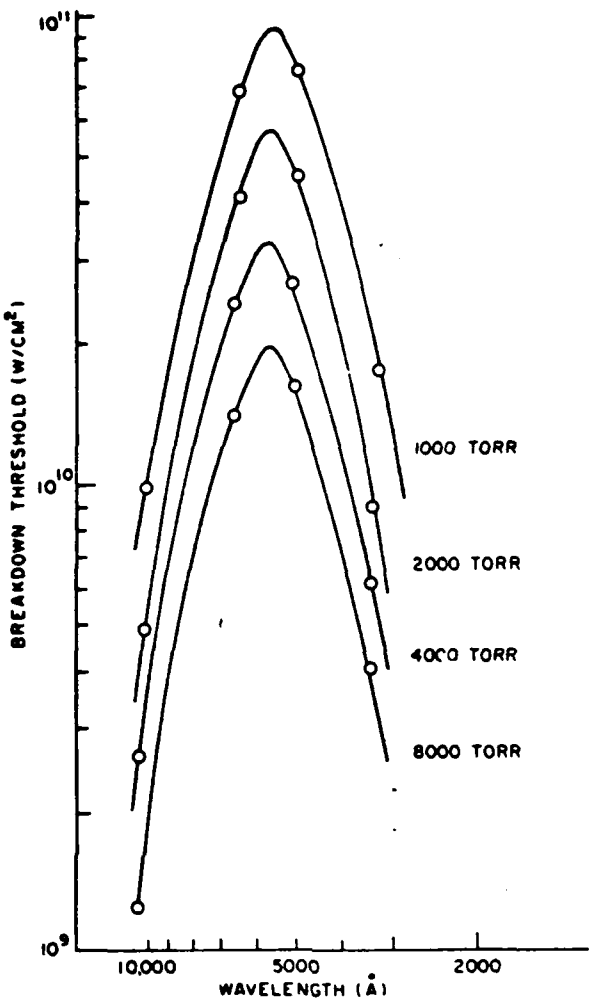

Fig. 11 Breakdown Threshold as a Function of Wavelength for Argon at Four Pressures (reprinted from Ref 17).

roughly equal to $f\theta$ = .01 cm, or the focal area is A = $\pi(.01)^2 = 3.14 \times 10^{-4}$. The resulting intensity, 3×10^{10} w/cm^2, is enough to cause gas breakdown within the Raman cell at even low pressures, and this was found true in the experiment.

III Equipment and Procedure

In this chapter the equipment and the experimental procedure used to obtain the results of Chapter IV are discussed. Both the equipment and the procedure evolved a great deal over the course of the experiment; only the final configurations are described here. The equipment will be described in the first section and the procedure will be described in the second section.

Equipment

This section on equipment will be divided into subsections describing each major component group: the ruby laser system, the Raman cell, the detectors, the R7912 transient digitizer, and the optical components. It should be noted that both the laser system and the R7912 transient digitizer performed unreliably during most of the experiment. Their peculiarities have added doubt to the accuracy of the stated results.

Ruby Laser. The excitation source for the Raman scattering was a Korad ruby laser system comprised of two K1 heads, two K25 10 kv power supplies, a KWC7 water cooler, and accessories. The two K1 heads served as oscillator and amplifier as shown in Figure (12). They were each fitted with a ruby rod 4 inches long and 1/4 inch in diameter. Since the amplifier was generally operated at higher voltages than the oscillator, the oscillator power supply

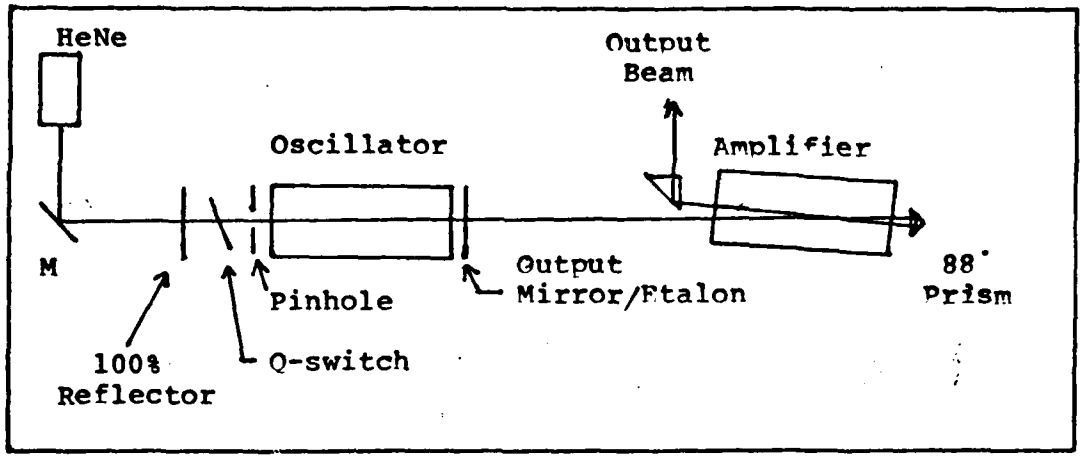

Fig. 12 Ruby Laser System.

was enslaved to the amplifier power supply so that both heads fired simultaneously. The dial voltage settings on the power supplies were calibrated with a high power digital voltmeter.

The oscillator was placed between a ∿100% reflecting rear mirror of four meter radius and a cooled Fabrey-Perot etalon and output mirror forming a cavity 27 cm in length. The etalon limited the longitudinal modes to a single mode. A pinhole of 1.7-2 mm in diameter was used to maintain single transverse mode operation. The laser oscillator was passively Q-switched by a mixture of cryptocyanide and methanol in a dye cell situated at the Brewster's angle within the cavity.

The output beam from the oscillator was made to double pass the amplifier using an 88° prism as shown in Figure (12). The final energy output of the system was from 90-200 mJ in a pulse width of 9-20 ns (FWHM). The maximum output power was about 12 MW with a spot diameter of ∿3 mm.

Divergence of 1 mrad was measured, and the linewidth was estimated to be .034 cm^{-1} from previous work with this laser system (Ref 18).

Raman Cell. The Raman cell was constructed of stainless steel tubing 6 feet in length, 1.25 inches (in) in inner diameter, and 1.5 inches in outer diameter. Inner end caps were welded to the tube and outer end caps were fastened to the inner caps with bolts. Fused quartz windows antireflection coated for 6943Å were sandwiched between the end caps cushioned by an inner O-ring seal and an outer teflon seal. The windows had a wedge of 30 minutes which helped eliminate multiple reflection effects. An internal lens one inch in diameter was mounted with spring strips to allow movement in the tube. The lens, with a focal length of 10 cm, was positioned 14 cm from the tube end farthest from the laser (the "front").

High pressure gas valves mounted near the front and rear ends of the tube were connected to a vacuum pump and a gas source, respectively. The gas pressure was controlled with a regulator and pressure meter with 10 psi increments. The gas cell could be cleared with a vent and pumped to near vacuum with the vacuum pump. The Raman cell was mounted on holders that could be adjusted vertically or horizontally to facilitate alignment. The cell was designed to withstand 40 atm of pressure with a safety factor of 10.

Detectors. Four detectors were used to monitor the input and output pulses. A Scientech 362 power/energy meter with a calorimeter head was used to determine the total energy of the pulse and to calibrate the other detectors. An ITT F4000 (SI) vacuum photodiode (VPD) powered by a Tullamore high voltage supply was used for accurate measurement of the reverse Stokes pulse. Its sensitivity at the Stokes wavelength (8704Å) and the Ruby wavelength (6943Å) was the same and equal to 8.25×10^{-4} A/W, and its rise time was 500 ps. The large detector area of the VPD (2.25 inches diameter) allowed easy placement of the detector and ensured capture of the entire beam. The VPD was isolated in a light tight box to avoid spurious signals and prevent accidental electric shock. A Lasermetrics 3117 photodiode (PD) and power supply with a 1 cm aperture was used to detect forward and incident (pump) pulses. It had a quoted sensitivity of .415 A/W at 6943Å and .5 A/W at 8704Å, and a rise time of 150 ps. A homemade PIN diode (P/N) was also used to monitor the forward and pump pulses. The P/N and the PD detectors yielded inconsistent amplitude results but were accurate for pulse width measurements. This was due to their small detector surfaces. Accuracy for power measurements was enhanced by recalibrating the detectors for each new experiment.

R7912 Transient Digitizer. The signals from the diode detectors were observed on a Tektronics R7912 Transient Digitizer (TD). The TD was used mainly as a storage scope to view pulse shapes. Photographs were taken of interesting pulses and saved for use in this report. The TD was fitted with a 7A29 amplifier with a 50Ω input impedance, and a 7B92 time base with a lowest scale of 500 ps per division. The overall time constant of the detector-scope system was about 500 ps. The TD was prone to fits of wild behavior, but gave consistent results most of the time.

Optical Components. The optical components used in this experiment were mirrors, prisms, lenses, and filters arranged as shown in Figure (13). The dichroic mirror (DM) was positioned at 45° to the pump pulse to direct the ruby pulse into the Raman cell. The dichroic mirror selectively reflects ruby light while allowing the reverse Stokes light to pass nearly unattenuated into the VPD. Filters (F) were used to further discriminate different frequencies. A ruby interference filter was used to select ruby and Brillouin light, and an RGN9 glass filter was used to select the Stokes light. The RGN9 filter has a transmission of .92 for Stokes (8704 Å) and 10^{-4} for ruby (6943 Å) and Brillouin frequencies. Neutral density filters were used to bring power down to levels acceptable to the detectors. The neutral filters added uncertainty to power measurements, perhaps as much as a factor of two. Negative lens L2 was used to expand the reverse pulse before it

entered the VPD, and lens L3 was used to recollimate the forward pulse before it traveled to its detector. The forward pulse was observed either directly by the PIN diode or by the VPD after a set delay of path B. A spectra physics HeNe laser passed through the ruby system via mirror M3 was used to align the system.

Experimental Procedure

The experimental procedure was designed to determine the characteristics of the Raman cell output pulses. Of most importance and relevance was the reverse Stokes pulse, which was studied in detail. Other pulses were observed in a qualitative fashion to determine their effect on the Stokes output. The forward transmitted pulse, for example, should show signs of depletion if the reverse Stokes pulse is strong or gas breakdown occurs. The experimental section is divided into four subsections: alignment, energy and pulsewidth measurements, general observations, and gain/threshold measurements. The basic setup for all experiments is shown in Figure (13).

Alignment. The entire system was aligned with a HeNe laser beam passed through the ruby laser system. The laser oscillator was aligned first by centering the HeNe beam through both ends of the ruby rod using a movable HeNe mount and a movable mirror as shown in Figure (12). The rear mirror, Q switch, and 100% reflector were then added one at a time and their reflections made coincident with

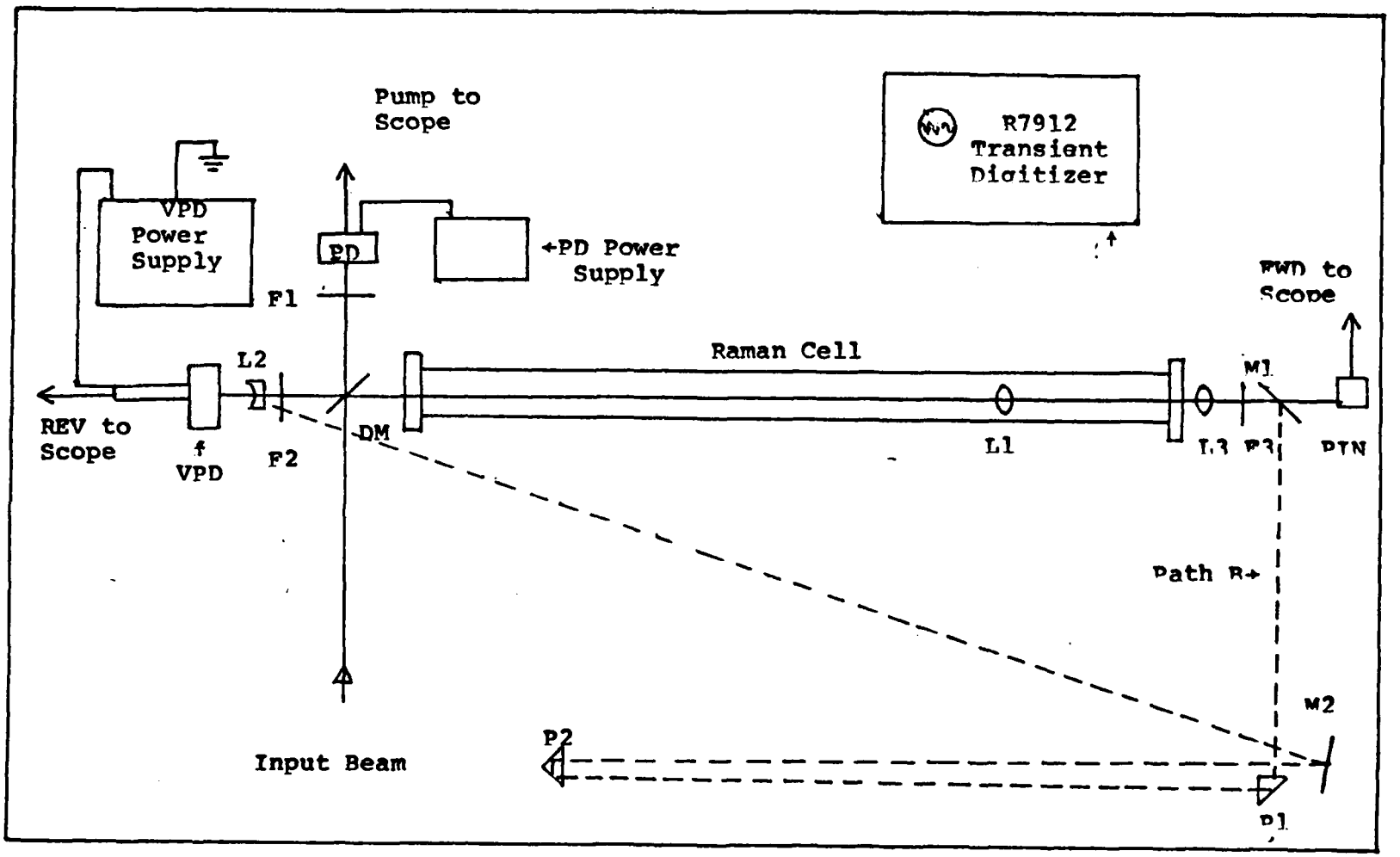

Fig. 13 Experimental setup for investigation of BSRS. Legend: DM-dichroic mirror; L1, L2, L3-lenses; P1, P2-prisms; F1, F2, F3-filters; VPD-vacuum photodiode; PD-photodiode; PIN-PIN diode.

the HeNe beam. The pinhole was then added and the laser fine tuned for maximum output and TEM_{00} mode structure. The mode structure was observed on burn paper. The HeNe beam was then adjusted to exactly match the ruby burn spot and the ruby amplifier was aligned to the HeNe beam as shown. Remaining components were aligned to the HeNe beam. The length of the output ruby pulse was controlled by changing the concentration of dye in the Q-switch.

Energy/Pulsewidth Measurements. The pulse length and pulse energy of the input pump pulse were monitored simultaneously by replacing the Raman cell in Figure (13) with the Scientech calorimeter head. The beam was expanded four times with a plano-concave lens to avoid damaging the calorimeter surface. Pulse width was monitored on the TD using the PD detector in the pump position. Energy/pulsewidth measurements were made before each experiment to determine the characteristics of the input pulse. As only one storage scope (the TD) was available, simultaneous and accurate monitoring of more than one pulse was impractical. A reflected pump pulse often was present with other pulses, but only relative changes in intensity were measured this way. The absolute intensity of the pulses was determined by relating to the known input pulse energy and pulse width.

General Observations. Observations of the output pulses at the three detectors were made as gas

pressure and laser input power were varied. This phase of the experiment was preliminary in nature and designed to see what kind of pulses could be observed. Later, better controlled experiments were conducted to take quantitative data. The average characteristics of the pump pulse were determined as above. With this pump pulse, the reverse pulses were monitored while gas pressure was varied from a vacuum to 200 psi. The same test was carried out using the other detectors at the pump and forward locations (See Figure (13)). The laser input pulse was then changed and the process repeated. The spectral content of the output pulses was checked by inserting a ruby interference filter or the Stokes selective RGN9 filter into the beam path. The dependence of the output pulses on input power at a given pressure was observed in the same way. The absolute energies of the output pulses were checked by replacing the appropriate detector in Figure (13) by the calorimeter head.

Timing measurements were made in the reverse direction by noting the pulse separation of observed Stokes and Brillouin pulses from the reflected pump pulse. At high intensities the pump reflection was drowned out and a new method used. The forward pulse was directed into the VPD via path B in Figure (13). Since the transmitted forward pulse had a sharp, distinctive edge (see the following Chapter) it made a convenient reference signal. The Stokes or Brillouin pulses could then be filtered and passed into the VPD along with the forward reference pulse. The pulse

separation was measured as a function of pressure from 0-200 psi.

Gain/Threshold Measurements. This more controlled portion of the experiment was designed to determine the power threshold for BSRS as a function of pressure and the BSRS gain. The input laser energy was set to the maximum for TEM_{00} mode (~126 mJ). At several pressure settings, the reverse Stokes pulse was monitored as the input energy was decreased by placing glass slides into the beam. Slides were added until the Stokes pulse was no longer observed. The gas tube was then replaced by the calorimeter head and the measured energy was taken as the threshold for BSRS at that pressure. The Stokes output at constant input energy of 126 mJ was also determined as a function of pressure and measurements of Stokes output at a given pressure as a function of input energy were made. This data was used to estimate the BSRS gain. The movement of the tube in this method introduced some error.

IV Results and Analysis

The results presented in this chapter give the reader insight into the kinds of output pulses that can be expected from a Raman cell and present quantitative data on their variation with gas pressure and laser power. From this information an operating range can be determined in which the reverse Stokes pulse is optimized. The results are applicable only to similar Raman systems, and they are limited in accuracy to a factor of two due to experimental problems. The general output characteristics are described first. Then each output pulse and its power and pressure dependence are analyzed closely.

General Output Characteristics

The intensity of the output pulses was strongly dependent on the input intensity, but the type of pulse observed was more dependent on pressure. In general, the output intensity increased with input intensity and the number of output pulses observed per each input pulse increased with pressure. The three basic pulse groups observed were the incident pump and depleted (transmitted) pump pulses, the forward and reverse Stokes pulses, and the reverse and reamplified Brillouin pulses.

The pulses observed in three pressure regimes are shown in Figure (14) for an input energy of ∿100 mJ. At pressures very close to 9 psi the input pulse of ∿12 ns FWHM was observed at all three detector locations (see Figure (13) for detector locations). The pump pulse seen in

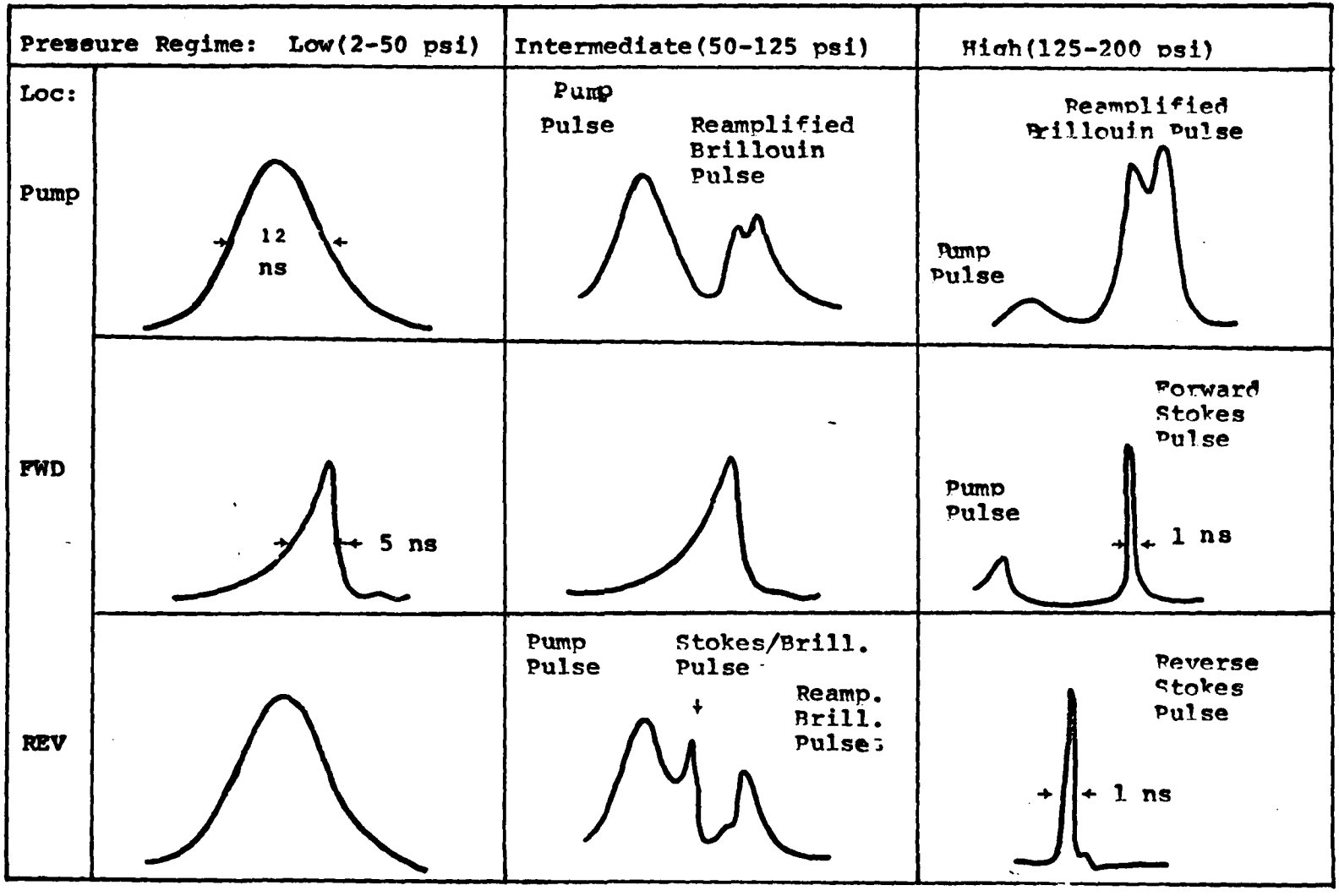

Fig. 14 Pulse Shapes in Three Pressure Regimes. Vertical scale is power, horizontal is time. (Not to scale).

the reverse direction was a reflection from the rear window of the Raman cell. At pressures greater than 2 psi, strong absorption of the incident energy led to the depleted 5 ns forward pulse. Reverse Brillouin and Stokes pulses as well as reamplified Brillouin pulses began to appear at pressures in the intermediate range of 50-125 psi. In this range, the Brillouin pulse was much greater than the Stokes pulse. The reamplified Brillouin pulse was reflected by the dichroic mirror and retraversed the laser system and was, therefore, detected at both the pump and reverse detector locations. In the high pressure regime (125-200 psi), the Brillouin and Stokes pulses grew to intensities comparable to the pump intensity. The reverse Stokes pulse was less than 1 ns wide, while the Brillouin pulse was 3-5 ns in width. The reamplified Brillouin pulse exceeded the initial pump power by as much as eight times and was intense enough to create a second reverse and/or a forward Stokes pulse. These Brillouin pumped pulses were seen intermittently. The time sequence of events that led to the identification of the output pulses is presented in Appendix II. A detailed description of each pulse follows.

Detailed Pulse Descriptions

In this section each pulse is examined closely and its origins are explained. The initial pump pulse is described first followed by output pulses in order of their appearance as pressure increased. The power vs. time plots of

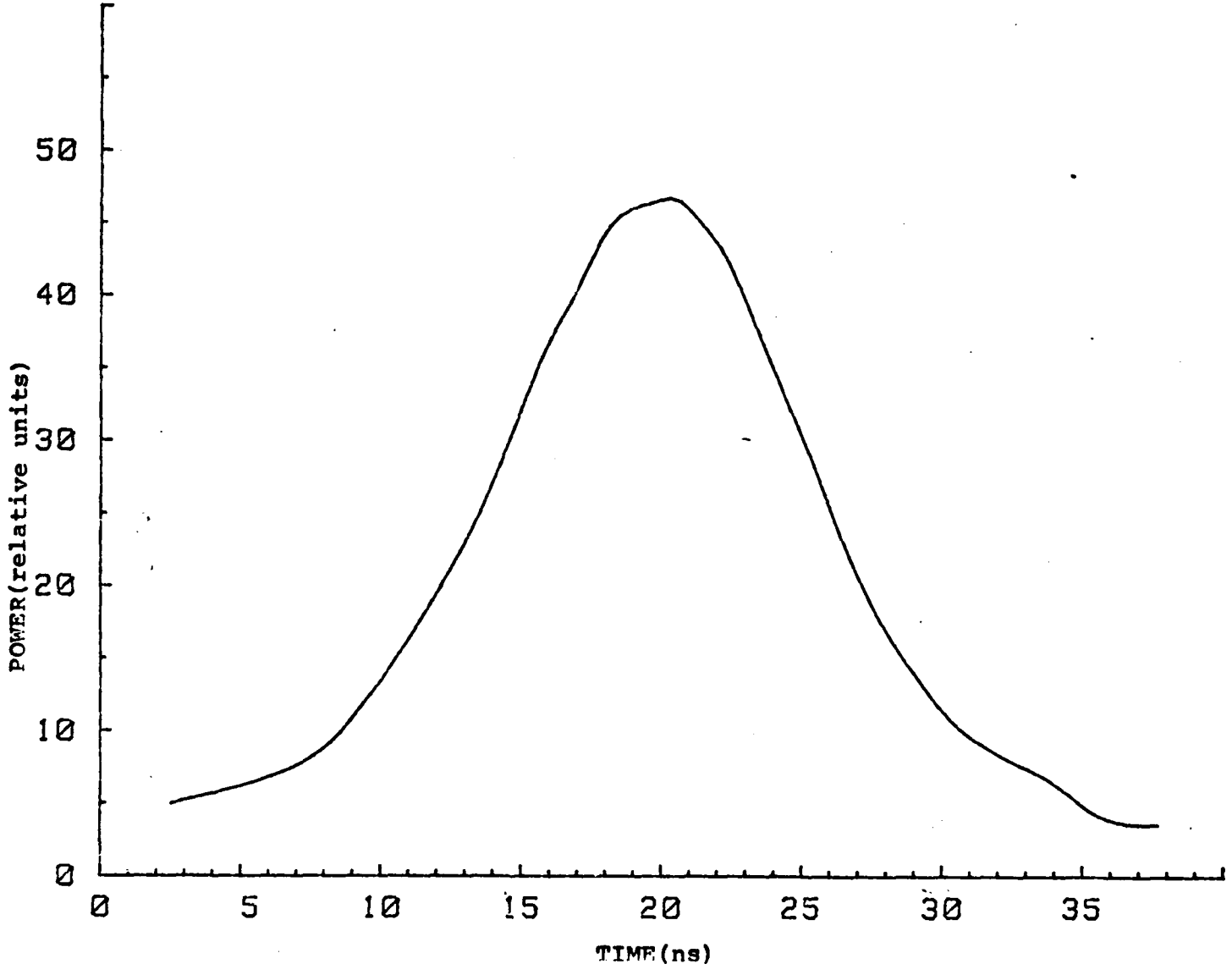

Fig. 15 Typical pump pulse. The peak power is 14 MW.

each pulse were created by computer tracing of an oscilloscope photograph.

Pump Pulse. A typical pump pulse is shown in Figure (15). The pulse shape is Gaussian with a width of 12.5 ns (FWHM) and a peak intensity of 14 MW. For this plot, the laser oscillator pinhole size was 2 mm, and the output mode was TEM_{00}. The input pulse width varied from 9-20 ns and the peak power varied from 10-25 MW. The corresponding input energy range was 80-200 mJ.

Depleted Pump Pulse. The depleted pump pulse appeared at pressures as low as 2 psi. A typical depleted pump pulse, henceforth referred to as the forward pulse, is shown in Figure (16). The plot was made at 100 mJ input energy and a pressure of 10 psi. The forward peak power is 2.5 MW and the pulse width is 5.5 ns. No other emission was observed from the Raman cell to compensate for the 90% loss of input energy. It is suspected that gas breakdown is responsible for this loss of energy. Since re-emitted light from gas breakdown is random in direction, it is not surprising that no emission was observed. Other evidence supporting this explanation follows.

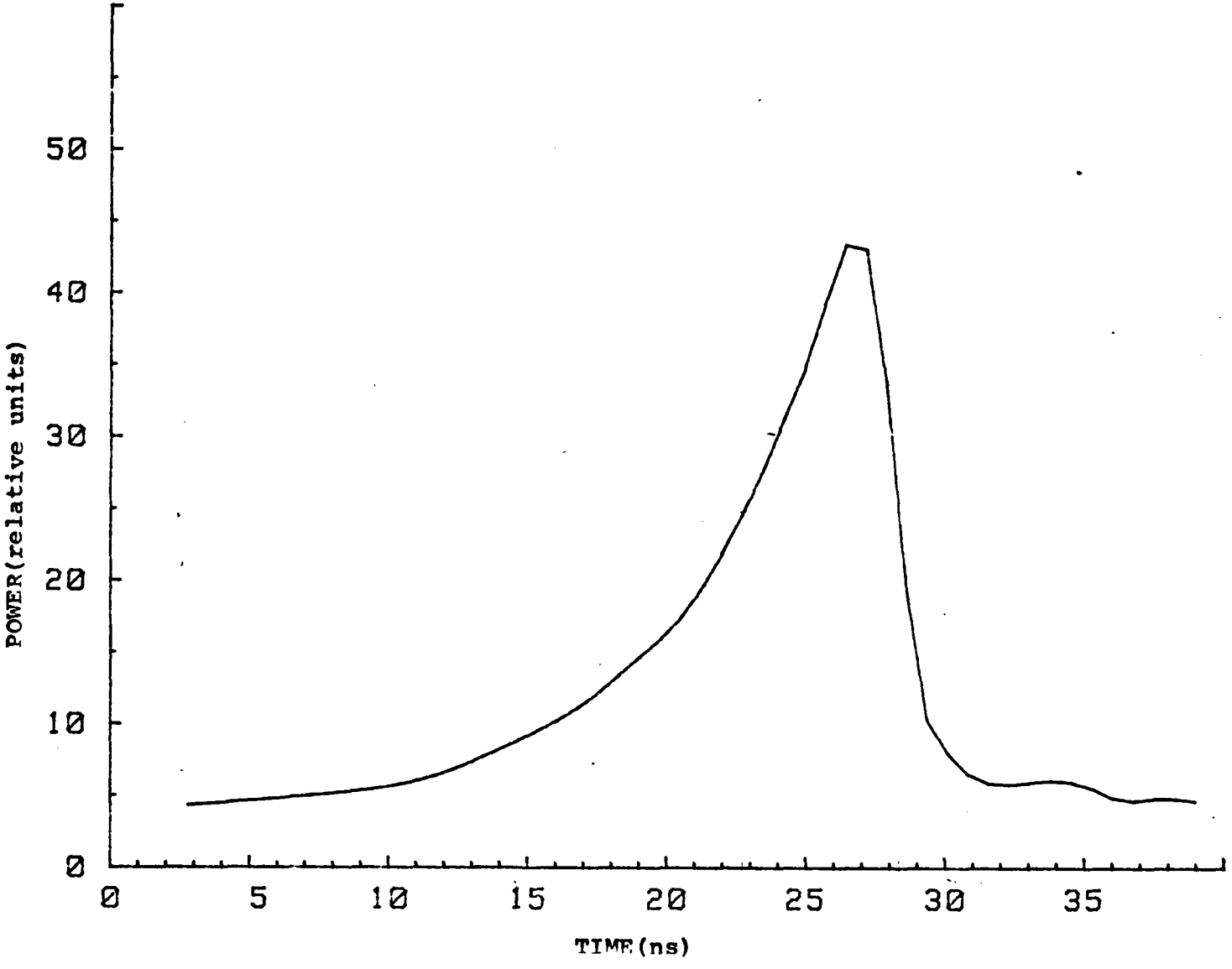

Fig. 16 Depleted Pump Pulse at 10 psi and 100 mJ. The peak power is 2.5 MW.

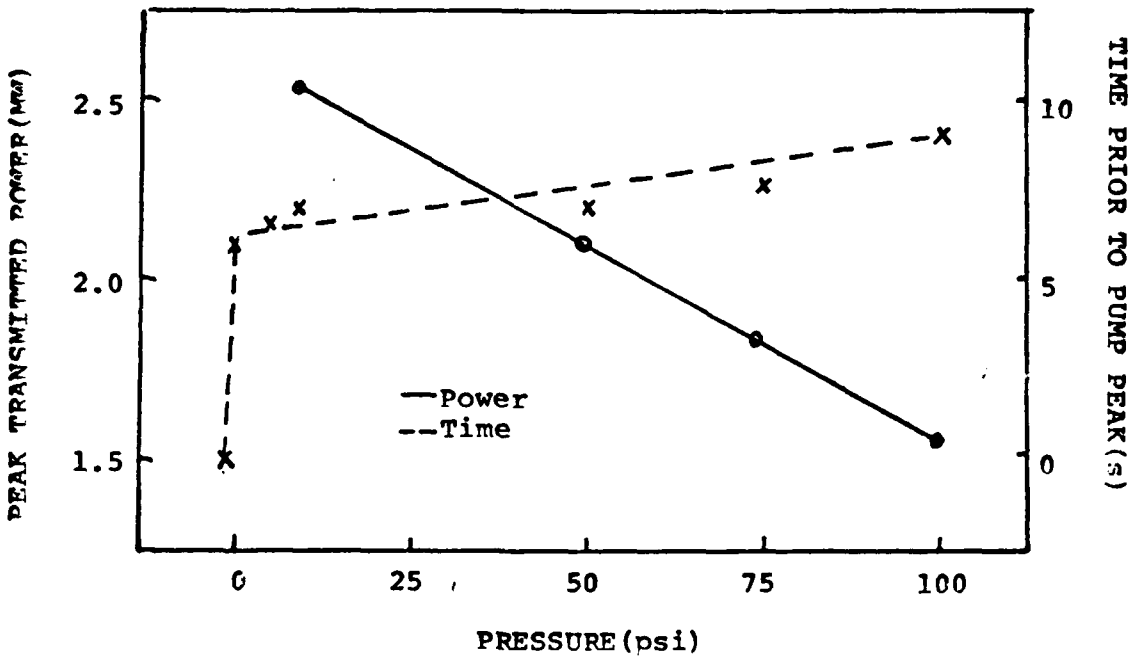

Fig. 17 Peak Transmitted Power and Time to Breakdown vs. Pressure

The forward transmitted peak power and peak position in reference to the pump peak at vacuum are plotted in Figure (17). The peak power transmitted at 0 psi was 14 MW, but was drastically reduced as soon as the pressure was measurable and then decreased linearly with pressure. This behavior is expected for gas breakdown (see Figure (10)). The time to breakdown is equal to the time prior to pump peak minus the halfwidth of the pump pulse. Although the front edge of the pump pulse is not well defined, one can see from Figure (17) that the time to breakdown decreases linearly with pressure. This is yet another indication of the decreasing threshold dependence on pressure.

The energy transmitted was also measured as pressure was increased, and similar results were obtained. The

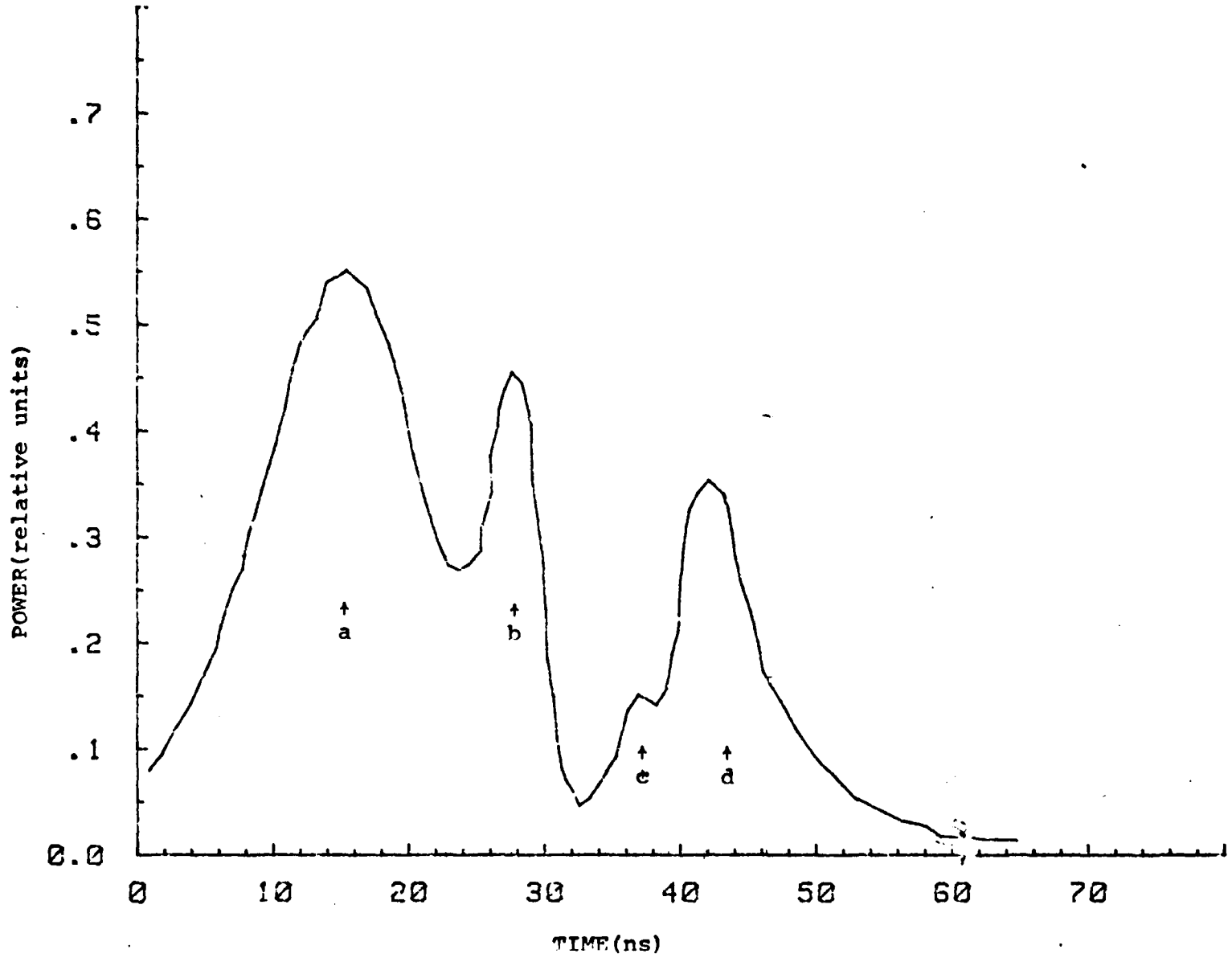

Fig. 18 Filtered Reverse Output at 125 psi and 92 mJ.

transmitted energy was 10% of the total pump energy. The great energy loss due to breakdown was responsible for lowering the efficiency of the BSRS process and also for introducing unknown anomalties to the Raman cell output. The reverse Stokes pulse is generated much more quickly than breakdown, however, so the reverse pulse can move into the pump pulse and be amplified before breakdown occurs. The forward emission increased at pressures above 100 psi due to the generation of other pulses.

Reverse Brillouin Pulse. The Raman cell output in the reverse direction (filtered to eliminate the Stokes component) is shown in Figure (18). The first pulse (a) is the reflection of the pump pulse from the rear window of the gas cell. The pump pulse for this case had a peak intensity of 11 MW and a pulsewidth of 15 ns. Pulse (b) is the reverse Brillouin pulse separated from the pump pulse by 13 ns, the time required for the pump pulse to travel 6 feet into the tube, stimulate the Brillouin process, and return 7 feet to the detector. The Brillouin pulse (b) should not be compared directly to the pump pulse (a) because the Brillouin pulse travels directly into the detector while the pump pulse is a reflection. The ruby reflectance of the window is .01 so that the peak Brillouin power is 90 KW; the width of pulse (b) is 5 ns. Observed Brillouin pulses varied in width from 3-6 ns.

The dependence of the Brillouin peak power on pressure at an input power of 20 MW is plotted in Figure (19). The output power increases nearly exponentially with pressure as

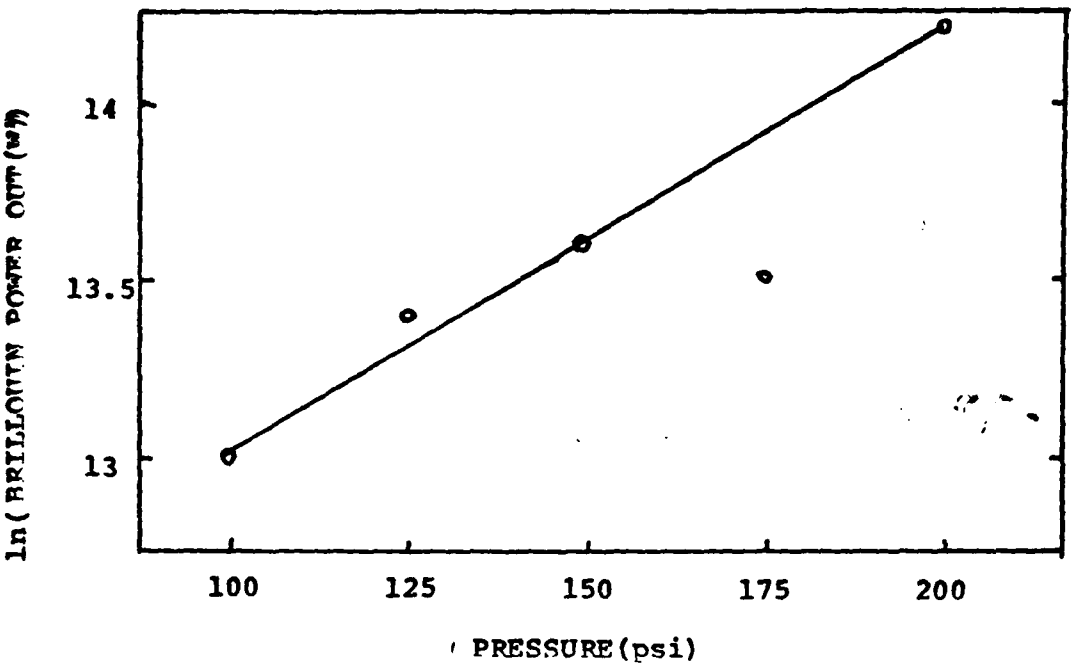

Fig. 19 Peak Brillouin Power vs. Pressure.

expected from theory. The large swing in values from the line is due most likely to experimental errors. Figure (19) can be compared to Figure (9) of Chapter II. The linear increase in gain depicted in Figure (9) indicates that the Brillouin output should be exponential as shown in Figure (19). Reverse Brillouin pulses as great as 1.5 MW were observed at 200 psi. This is the pressure at which the Brillouin gain becomes equal to the Raman gain according to Figure (9). At pressures above 200 psi the pump energy was preferentially funneled into the Brillouin pulse. The maximum energy of the Brillouin pulse was only 5 mJ, however, so the fraction of pump energy lost to Brillouin scattering was less than 5%.

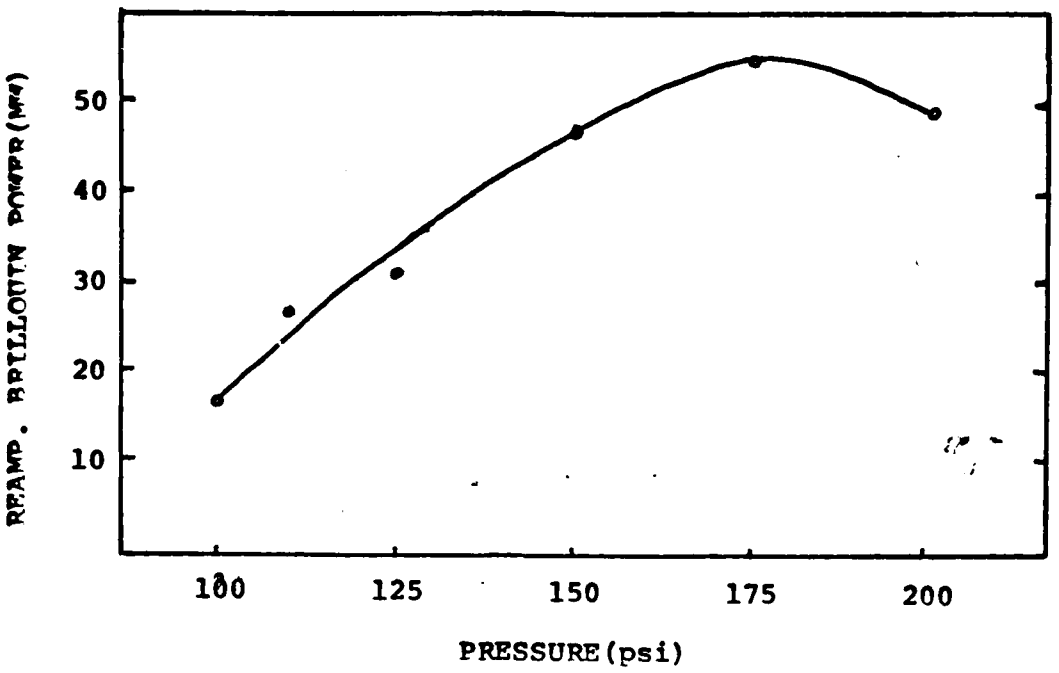

Fig. 20 Reamplified Brillouin Peak Power vs. Pressure.

Reamplified Brillouin Light. Reamplified Brillouin pulse (c) occurs 9 ns after the reverse Brillouin pulse. This time corresponds to the transit time through the laser system and back to the detector. The second reamplified pulse (d) is delayed by 4 ns because it makes an extra round trip through the laser oscillator. This also explains its greater magnitude. Since the reamplified pulses follow the same path as the pump pulse, they may be compared to it directly. The peak power of pulse (d) is then 7 MW, and its width is 7 ns.

The dependence of the second reamplified Brillouin power on pressure is plotted in Figure (20). The power increases to as much as 55 MW after which no more photons may be swept from the laser system and the power levels off. The reamplified Brillouin light also re-entered the Raman

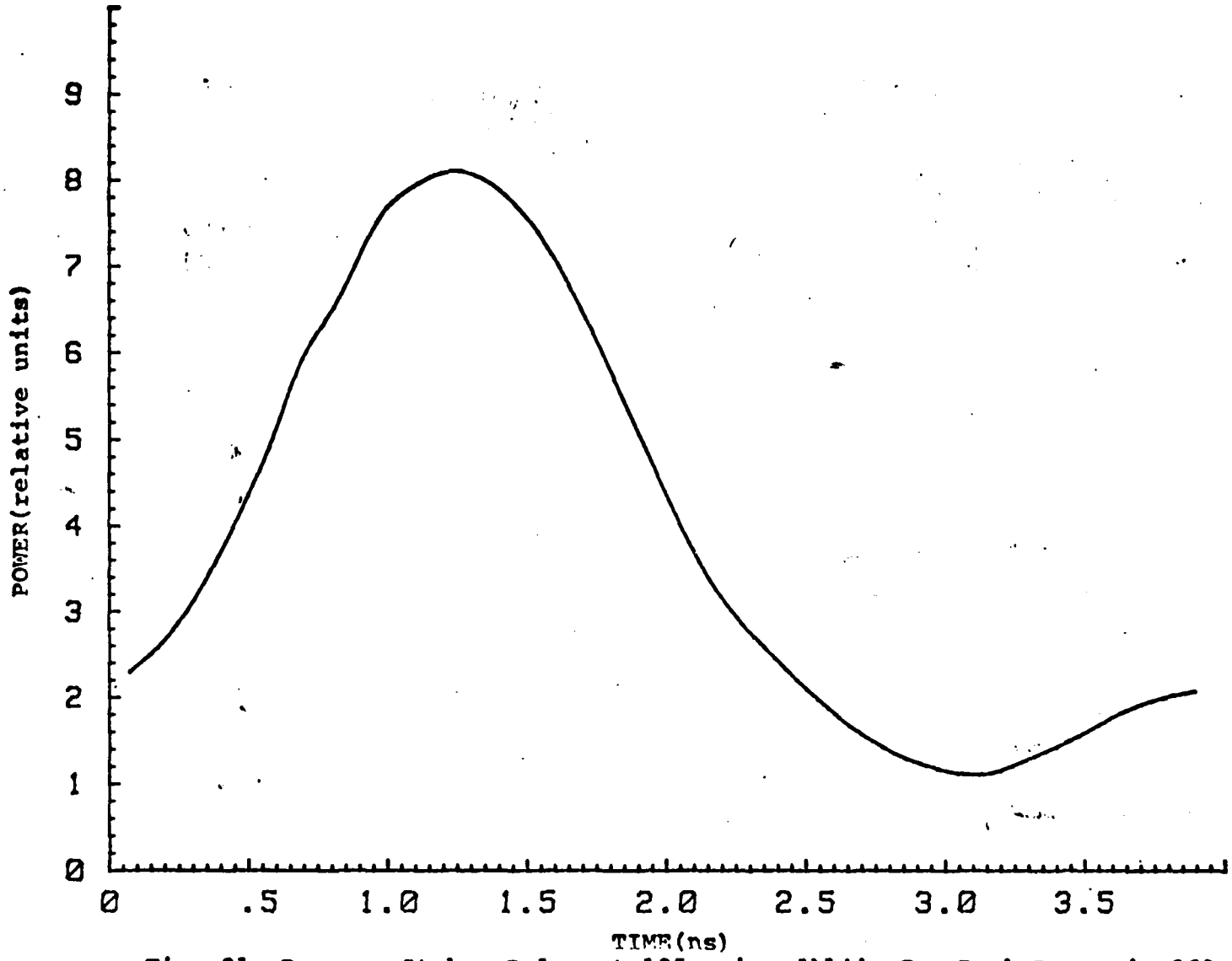

Fig. 21 Reverse Stokes Pulse at 125 psi and 144 mT. Peak Power is 360 KW.

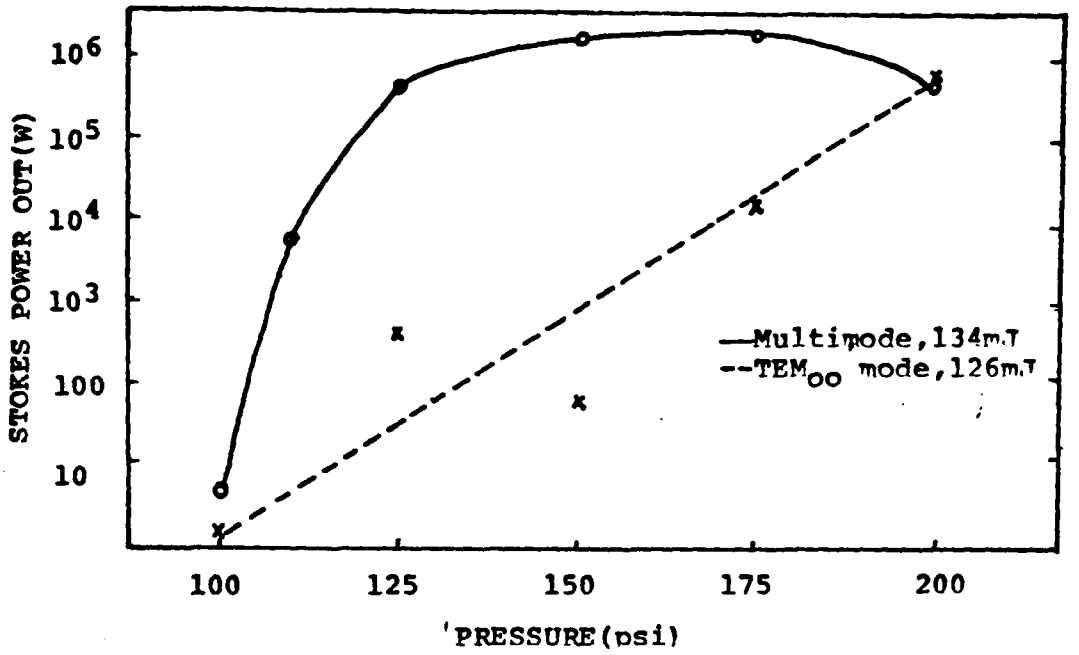

Fig. 22 Stokes Output vs. Pressure.

cell and served as a pump pulse for a second round of scattering processes. The reamplified light was usually absorbed or scattered completely by the gas breakdown process, but occasionally produced its own reverse Stokes and Brillouin pulses and/or a forward Stokes pulse. Because of this, the reamplified Brillouin pulses were quite interesting.

Reverse Stokes Pulse. The reverse Stokes pulse (Raman pulse) appeared strongly at pressures above 125 psi and input powers above 5 MW. Timing measurements described in Chapter II were used to determine that the reverse Stokes and Brillouin pulses occurred within one nanosecond of each other. The time to the scattering threshold was seen to decrease with pressure. A typical reverse Stokes pulse is shown in Figure (21). This plot was made at 125 psi with

an input power of 20 MW and an input pulsewidth of 13 ns. The Stokes pulse shown has a peak power of 360 KW and a pulsewidth of 1.5 ns. Other Stokes pulses were observed with peak powers of up to 15 MW at 150 psi. This high powered Stokes pulse was produced from a 30 MW pump pulse with a width of 9.5 ns. The smallest observed pulsewidth was 800 ps; this value was limited by the response time of the equipment. Second reverse Stokes pulses separated from the first by 30 ns, were observed at times, but they were too weak to be of any use.

The dependence of the reverse Stokes peak power on pressure for two input powers is shown in Figure (22). The dashed line was produced with an input pulse of 126 mJ total energy, 16 ns pulsewidth, and 14 MW peak power. For this case the laser oscillator was fitted with a 1.7 mm aperture to insure TEM_{00} mode. The large variations were due to movement of the tube between data points. Small signal conditions were assumed for the straight line, but the validity of this assumption is marginal. The saturation fluence, S, given by equation (13), is equal to 544 $J/cm^2 \cdot P$, where P is the pressure in atmospheres. The output Stokes pulse had a transverse beam diameter of 3 mm, and a maximum energy of 0.4 mJ at 200 psi. At this pressure, the Stokes fluence was 50 J/m^2 while the saturation fluence was 40 J/m^2, so that saturation would be expected to occur at 200 psi. Below this pressure the Stokes output power should roughly obey equation (34) for exponential gain. From the dashed line, the gain constant

is C = 1.86 P. The pump fluence for the pump pulse energy of 126 mJ with a beam diameter of 5 mm is 1.6×10^3 J/m^2. Using this value in equation (13) leads to a gain coefficient, $\gamma = 7.76 \times 10^{-12}$ M/W. This value is only slightly smaller than the theoretical value given by equation (41), 9.76×10^{-12} M/W, and is certainly within the experimental accuracy.

The solid line in Figure (22) is the Stokes output power for a pump pulse 12 ns in width, 134 mJ in total energy, and 20 MW in peak power. A 2 mm aperture was fitted into the laser oscillator to increase the energy, and resulted in an imperfect mode structure. The sharper starting slope of this plot is due to the great increase in initial Stokes intensity from the previous case. The curve peaks at 2 MW at 175 psi, after which it levels off due to saturation and competing processes. The output Stokes in this case had a peak energy of 1.4 mJ and a saturation fluence of 226 J/m^2. Thus, it is reasonable to expect saturation to occur earlier in this case than the previous one.

The Stokes output at both energy values was limited by competing nonlinear processes more than by saturation. The competing processes were especially great above 200 psi where Brillouin gain exceeds the Raman gain and gas breakdown is more intense. High input powers also aggravated the competition problem.

The Raman scattering threshold energy as a function of pressure is shown in Figure (23). The threshold decreased with pressure in a nearly linear fashion. The bad data point at 125 psi is due to movement of the tube between data points.

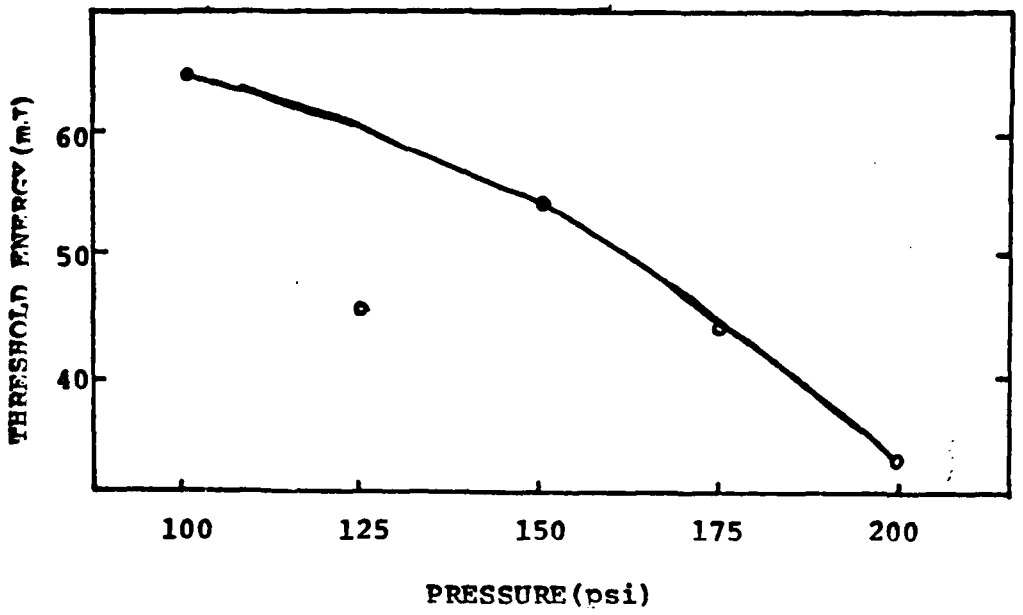

Fig. 23 Raman Threshold vs. Pressure.

This plot can be compared to Figure (9) which also shows how the threshold decreases and hence the gain increases with pressure.

Near threshold, the Stokes pulse output had a Gaussian shape and only single Stokes pulses were observed. At higher pressures multiple pulses were sometimes seen with separations of 0.8-6 ns. The multiple pulse structure was more prominent when the input mode structure was imperfect. Plots of these pulse shapes are presented in Appendix III. The single reverse Stokes output was optimized in terms of power and pulsewidth in the 150-175 psi range at powers from 125-160 mJ. The multimode structure of the input pulse required to obtain energies more than 140 mJ caused a broadening of the observed Stokes pulse to 1.5 ns from its optimum width of 0.8 ns with TEM_{00} mode input. Operation at values lower than those in the optimum range caused a drastic reduction in output. Operation at higher values

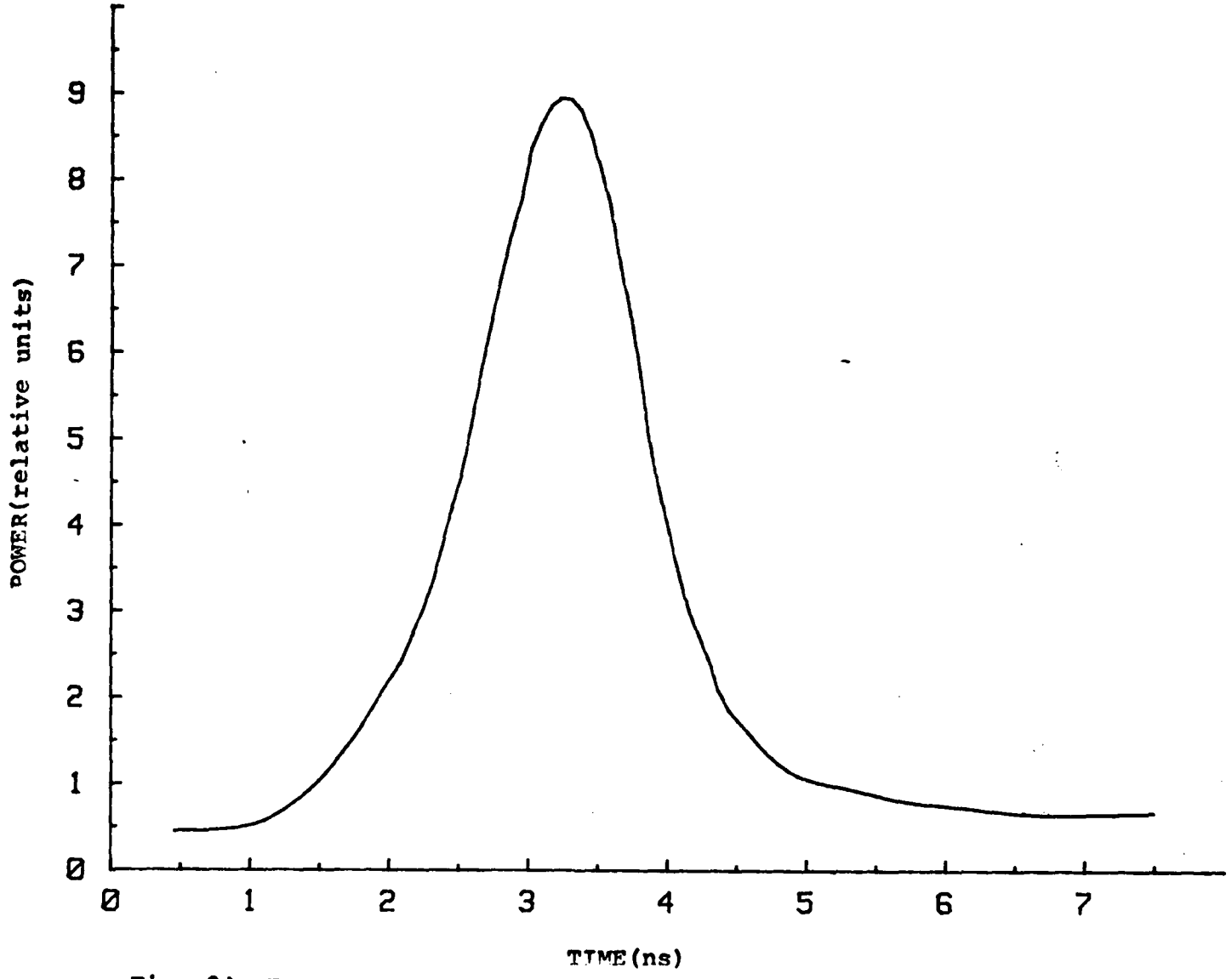

Fig. 24 Forward Stokes Pulse at 160 psi and 92 mJ. Peak power is 4MW.

also caused a decrease in the average Stokes power. High power operation produced the most intense Stokes pulses, but the output power fluctuated wildly and contained a high proportion of unwanted Brillouin light. Multiple Stokes pulses and gas breakdown accompanied by loud snapping noises also prevented efficient operation in a higher power or pressure range.

Forward Stokes Pulse. A forward Stokes pulse with powers typically greater than 1 MW was also seen from time to time. The forward Stokes pulse grew from the reverse Stokes remnants left in the reamplified Brillouin light. It was observed only at pressures above 160 psi. A typical forward Stokes pulse is shown in Figure (24). It has a peak intensity of 4 MW and a pulsewidth of 1.5 ns. The plot was made with an input pulse of 15 MW peak power and 11 ns in width. The observation of a forward Stokes pulse seemed to require TEM_{00} mode structure, powers greater than 15 MW and pressures greater than 160 psi, as well as some unknown parameter such as tube alignment. Since all forward pulses are generally absorbed by the gas breakdown, it is surprising that a forward Stokes pulse is ever observed.

V Conclusions

A ruby pumped methane Raman cell was built and tested. The following conclusions can be drawn from the results presented in this report:

1. Reverse Raman Stokes pulses of up to 15 MW in peak power and less than 0.8 ns in width (FWHM) can be produced with this system. The maximum observed energy of the Stokes pulse was 10% of the pump energy. Such pulses are useful for other experimental work such as diffusion measurements.
2. This optimum performance of the Raman system was obtained at gas pressures of 150-175 psi and input laser energies of 125-160 mJ.
3. The efficiency of the Stokes conversion was limited by the competing processes of stimulated Brillouin scattering and gas breakdown.
4. The observed behavior of the Stokes pulse did not contradict theoretical predictions based on an injected input Stokes pulse. A measured small signal gain of 7.76×10^{-12} M/W was within 25% of the predicted value of 9.76×10^{-12} M/W.
5. Reamplified Brillouin light with peak pulse powers of 50 MW was responsible for producing a forward Stokes pulse 4 MW in peak power and 1.4 ns in width.

VI Future Work

The backward stimulated Raman scattering pulse compression scheme has been made operational at the Aero-Propulsion Laboratory at Wright-Patterson AFB. The output pulses may now be used in other experiments. Of particular interest to the lab is the measurement of the diffusion rate of GaAs using the short Stokes pulse. The diffusion rate can be determined by measuring the pulse spread due to recombination fluorescence. A KDP* frequency doubling crystal is in place at the lab and will be required to obtain photons with energies high enough to create electron-hole pairs on the surface of the GaAs.

Since the accurate measurement of the Stokes pulsewidth was not possible during this investigation, the autocorrelation technique might be used to measure the Stokes pulsewidth. In this method the pulse to be measured is separated into two perpendicularly polarized waves. A small accurately measured path difference is then introduced between the two before they are directed into the crystal. Since the crystal requires one photon from each polarization direction to create a single frequency doubled photon, the frequency doubled output will depend on the overlap of the two input pulses. The spread in second harmonic power as the path length is varied leads to an accurate determination of the pulsewidth.

Bibliography

1. Carman, R. L., F. Shimizu, C. S. Wang, and N. Bloembergen. "Theory of Stokes Pulse Shapes in Transient Stimulated Raman Scattering," Physical Review, A2: 60-72 (July 1970).

2. Culver, W. H., T. A. Vanderslice, and V. W. T. Townsend. "Controlled Generation of Intense Light Pulses in Reverse Pumped Raman Lasers," Applied Physics Letters, 12: 189-190 (1 March 1968).

3. Glass, Alexander J. "Design Considerations for Raman Lasers," IEEE Journal of Quantum Electronics, QE-3: 516-520 (November 1967).

4. Hellwarth, R. W. "Theory of Stimulated Raman Scattering," Physical Review, 130: 1850-1852 (1 June 1962).

5. Hon, David T. "Pulse Compression by Stimulated Brillouin Scattering," Journal of the Optical Society, 70: 1403-1404.

6. Kachen, G. I. Jr. and W. H. Lowdermilk. "Direct Observation of Subnanosecond Pulsations in Stimulated Raman Scattering," *IEEE Journal of Quantum Electronics*, QE-10: 746-747 (Sept 1974).

7. Kaiser, W. and M. Maier. "Stimulated Rayleigh, Brillouin and Raman Spectroscopy," Laser Handbook, Volume 2, F. T. Arecchi and E. O. Schulz-Dubois, Eds. Amsterdam, The Netherlands, North-Holland, 1972.

8. Kelley, P. L. and T. K. Gustafson. "Backward Stimulated Light Scattering and the Limiting Diameters of Self-Focused Light Beams," Physical Review A, 8: 315-318 (July 1973).

9. Maier, M., W. Kaiser, and J. A. Giordmaine. "Intense Light Bursts in the Stimulated Raman Effect," Physical Review Letters, 17: 1275-1277 (26 December 1966).

10. ----- "Backward Stimulated Raman Scattering," Physical Review, 177: 580-599 (10 January 1969).

11. Maier, M. "Applications of Stimulated Raman Scattering," Applied Physics, 11: 209-231 (July 1976).

12. Minck, R. W., E. E. Hagenlocker, and W. G. Rudo. "Simultaneous Occurrence and Competition Between Stimulated Optical-Scattering Processes in Gases," Journal of Applied Physics, 38: 2254-2260 (April 1967).

13. Murray, J. R., J. Goldhar, and A. Szoke. "Backward Raman Gain Measurements for KrF Laser Radiation Scattered by CH_4," Applied Physics Letters, 32: 551-553 (1 May 1978).

14. Murray, J. R., J. Goldhar, D. Eimerl, and A. Szoke. "Large Signal Gain and Intensity Enhancement in a Backward Raman Amplifier," Applied Physics Letters, 33: 399-401 (1 September 1978).

15. ----- "Raman Pulse Compression of Excimer Lasers for Application to Laser Fusion," IEE Journal of Quantum Electronics, QE-15: 342-368 (May 1979).

16. Perry, B., et al. "Controllable Pulse Compression in a Multiple-Pass-Cell Raman Laser," Optics Letters, 5: 288-290 (July 1980).

17. Ready, John F. Effects of High Power Laser Radiation (213-272), New York: Academic Press, 1971.

18. Roh, Won B. Coherent Anti-Stokes Raman Scattering of Molecular Gases, Technical Report AFAPL-TR-77-47. Wright-Patterson AFB, Ohio: Aero Propulsion Laboratory, August 1977.

19. Shen, Y. R. and N. Bloembergen. "Theory of Stimulated Brillouin and Raman Scattering," Physical Review, 137: 1787-1805 (15 March 1965).

20. Trenholme, J. and K. Munes. "A Simple Approach to Laser Amplifiers," Lawrence Livermore Lab. Rep. UCRL 51413, 1972.

21. Yariv, A. Introduction to Optical Electronics, New York: Holt, Rinehart and Winston, 1976.

Appendix I

This appendix is presented in two sections: the first section details the semiclassical derivation of the nonlinear polarization and the second section uses this result in Maxwell's wave equation to derive the radiation transfer equations. A two level vibrational system in which a molecule interacts with a linearly polarized electric field will be the model for this discussion. Spatial averaging will be ignored. The model does not take beam focusing into account.

Nonlinear Polarization

When a linear molecule with a dipole moment is subjected to a time-varying electric field, that molecule will experience a change in charge separation, q(t), proportional to the field strength. The polarization is the dipole moment per unit volume given by

$$P(t) = -Neq(t) \tag{45}$$

where N is the number of oscillators per unit volume and e is the charge of an electron. For very high fields the displacement and hence the polarization are no longer proportional to the electric field E.

The nonlinear contribution can be expressed using the susceptibility tensor χ in the frequency domain as

$$P(t) = \chi^{(1)}E(t) + \chi^{(2)}E^2(t) + \chi^{(3)}E^3(t) \tag{46}$$

where the tensorial nature of χ has been suppressed. The squared term is associated with frequency doubling while the cubed term is responsible for two photon processes and stimulated scattering processes.

Alternatively, the polarization can be expressed in terms of the polarizability, $\alpha(q)$, which can be expanded in a Taylor series about q.

$$P(x,t) = N\alpha(q)E(x,t) = N(\alpha_o + \frac{\partial \alpha}{\partial q} q)E(x,t) \quad (47)$$

where only the first two terms have been kept. This form is convenient for further development. The second term on the right is the nonlinear term of interest for stimulated Raman scattering.

The quantum mechanical derivation proceeds by assuming a two level vibrational system represented by a perturbed simple harmonic oscillator.

The wave function, Ψ, is written as the superposition of two states, ϕ_0 and ϕ_1.

$$\Psi(x,t) = a_0(t)\phi_0(x,t) + a_1(t)\phi_1(x,t) \quad (48)$$

where $|a_0|^2$ and $|a_1|^2$ are the probabilities of finding the particle in state 0 or 1. The nonlinear polarization, $P^{NL}(x,t)$, is written

$$P^{NL}(x,t) = N \frac{\partial \alpha}{\partial q} q\, E(x,t) \tag{49}$$

$$\langle P^{NL}(x,t) \rangle = N \frac{\partial \alpha}{\partial q} E(x,t) \int \Psi^* q \Psi dq \tag{50}$$

$$= N \frac{\partial \alpha}{\partial q} E(x,t) \sqrt{\frac{\hbar}{2\mu\omega_{01}}} (\rho_{01}^* + \rho_{01}) \tag{51}$$

where the matrix elements of q are given from the simple harmonic oscillator model

$$\phi_n^* q \phi_m dq' = \sqrt{\frac{h}{2\mu\omega_{01}}} \begin{pmatrix} 0 & 1 \\ 1 & 0 \end{pmatrix} \begin{matrix} n = 0,1 \\ m = 0,1 \end{matrix} \tag{52}$$

Here μ is the reduced mass of the oscillator and ω_{01} is the vibrational frequency of the excited state. ρ_{01} is the transition probability defined by the density matrix as

$$\underset{\sim}{\rho} = \begin{pmatrix} a_0 a_0^* & a_0 a_1^* \\ a_1 a_0^* & a_1 a_1^* \end{pmatrix} \tag{53}$$

An expression for ρ_{01} can be found by manipulation of the time dependent wave equation using a slightly perturbed Hamiltonian,

$$H = H_0 + V \tag{54}$$

where H_0 is the unperturbed Hamiltonian and V is the perturbed potential due to the interaction between the electric field and the oscillating dipole.

$$V = -\frac{1}{2} \bar{P}^{NL} \cdot \bar{E} \tag{55}$$

An expression for ρ_{01} can be found by manipulating the wave equation and requiring orthonormal basis functions, ϕ_n. The time dependent wave equation is

$$i\hbar \frac{\partial \Psi}{\partial t} = H\Psi \tag{56}$$

The eigenequation for the unperturbed oscillator requires that

$$H_0\phi_n = U_n\phi_n \quad , \quad n = 0,1 \tag{57}$$

where $U_n = \hbar\omega_{0n}$ is the energy of the unperturbed state. Substitution of the wave function from equation (48) into (56) and the subsequent use of equation (57) leads to

$$H\Psi = i\hbar \frac{\partial a_0(t)}{\partial t} \phi_1 + i\hbar \frac{\partial a_1(t)}{\partial t} \phi_2 \tag{58}$$

Multiplication of equation (58) by $a_1^*\phi_0^*$ and integrating over space yields

$$\rho_{01}U_0 + \rho_{01}V_{00} + \rho_{11}V_{01} = i\hbar \frac{\partial a_0}{\partial t} a_1^* \tag{59}$$

where

$$V_{nm} = \int_s \phi_n^* V \phi_m \, ds \qquad \begin{matrix} n = 0,1 \\ m = 0,1 \end{matrix}$$

$$= -\frac{1}{2} \frac{\partial \alpha}{\partial q} E^2 \sqrt{\frac{h}{2\mu\omega_{01}}} \begin{pmatrix} 0 & 1 \\ 1 & 0 \end{pmatrix} \tag{60}$$

where equations (55) and (52) have been used. Multiplication of equation (58) by $a_0^* \phi_1^*$, integrating, taking the complex conjugate, and subtracting this result from equation (59) leads to

$$i \frac{\partial \rho_{01}}{\partial t} + \omega_{01}\rho_{01} + i\Gamma\rho_{01} = LE^2 \qquad (61)$$

where

$$L = \frac{(N_0 - N_1)}{2hN} \frac{\partial \alpha}{\partial q} \sqrt{\frac{h}{2\mu\omega_{01}}} \qquad (62)$$

and

$$\Gamma = \pi \Delta\nu_R$$

The damping term, Γ, is just the linewidth of the Raman transition and has been added phenomenologically. N_0, N_1, and N are the population densities in level 0 and level 1 and their total, respectively.

The electric field inside the Raman active medium can be described by the superposition of two fields; E_p is the pump laser field traveling in the positive x direction with frequency ω_p, while E_s is the Raman Stokes pulse traveling in the negative direction with frequency $\omega_s = \omega_p - \omega_{01}$.

$$\begin{aligned} E(x,t) &= E_s(x,t) + E_p(x,t) \\ &= \frac{1}{2}\{E_{s0}(x,t)\exp[i(\omega_s t + k_s x)] + cc\} \\ &\quad + \frac{1}{2}\{E_{p0}(x,t)\exp[i(\omega_p t - k_p x)] + cc\} \end{aligned} \qquad (63)$$

Here cc stands for complex conjugate, k_s and k_p are the wave vectors for Stokes and pump pulse, respectively, where $k_i = \frac{\omega_i}{c}$, c being the speed of propagation in the medium. In equation (63) the anti-Stokes components have been omitted since the anti-Stokes gain is much smaller than the Stokes gain. Also, the forward Stokes component has been omitted since the forward interaction length has been kept short, hence reducing forward gain (Ref 7).

Substituting equation (62) into equation (61) and keeping only those terms resonant in $\omega_{01} = \omega_p - \omega_s$ leads to

$$i\frac{\partial \rho_{01}}{\partial t}+\omega_{01}\rho_{01}+i\Gamma\rho_{01} = \left[E_{p0}E_{s0}^{*}e^{i(\omega t-kx)}+E_{p0}^{*}E_{s0}e^{-i(\omega t-kx)}\right]\frac{L}{2} \tag{64}$$

where the time and space dependence of the variables E_{p0}, E_{s0}, and ρ_{01} has been omitted for clarity, $\omega = \omega_p - \omega_s$, and $k = k_p + k_s$.

The solution to equation (64) is straightforward when the amplitudes of the fields, E_{p0} and E_{s0}, and the density matrix element, ρ_{010}, are assumed slowly varying and treated as constants. A further justified assumption is that of heavy damping, i.e.

$$\begin{aligned} i\Gamma\rho_{010} &>> \frac{\partial \rho_{010}}{\partial t} \\ E_{p0} &>> \frac{\partial E_{p0}}{\partial t} \\ E_{s0} &>> \frac{\partial E_{s0}}{\partial t} \end{aligned} \tag{65}$$

The solution to equation (64) is then

$$\rho_{01} = \frac{LE_{p0}E^*_{s0}}{2}\left\{\frac{e^{i(\omega t-kx)}}{\omega_{01}-\omega+i\Gamma}+\frac{e^{-i(\omega t-kx)}}{\omega_{01}+\omega+i\Gamma}\right\} \quad (66)$$

The second term on the right is nonresonant in ω and can be ignored.

Finally, substitution of equation (66) and equation (63) into equation (50) for the nonlinear polarization, p^{NL}, yields

$$P_p^{NL} = A\left[\frac{E_{s0}E_{p0}E^*_{s0}e^{i(\omega_p t-k_p x)}}{\omega_{01}-\omega+i\Gamma}+cc\right] \quad (67A)$$

$$P_s^{NL} = A\left[\frac{E_{p0}E^*_{p0}E^*_{s0}e^{-i(\omega_s t+k_s x)}}{\omega_{01}-\omega+i\Gamma}+cc\right] \quad (67B)$$

$$P_{AS}^{NL} = A\left[\frac{E_{p0}E_{p0}E^*_{s0}e^{i[(2\omega_p-\omega_s)t-(2k_p+k_s)x]}}{\omega_{01}-\omega+i\Gamma}+cc\right] \quad (67C)$$

$$P_{ss}^{NL} = A\left[\frac{E_{p0}E^*_{s0}E^*_{s0}e^{i[(\omega_p-2\omega_s)t-(k_p+2k_s)x]}}{\omega_{01}-\omega+i\Gamma}+cc\right] \quad (67D)$$

The separate frequencies have been split up for legibility: P_p^{NL} is the pump frequency component, P_s^{NL} is the Stokes component, P_{AS}^{NL} is the anti-Stokes component, and P_{ss}^{NL} is the secondary Stokes component. The constant, A, is given by

$$A = \frac{N_0-N_1}{16\mu\omega_{01}}\left(\frac{\partial\alpha}{\partial q}\right)^2 \quad (68)$$

where N_0-N_1 is the difference in number density of particles in states 0 and 1, μ is the reduced mass associated with the vibration, and $\partial\alpha/\partial q$ is the nonlinear term of the polarizability. Since the Stokes term at frequency ω_s and the pump term at frequency ω_p create by mixing the resonant frequency $\omega = \omega_p - \omega_s \simeq \omega_{01}$, these two terms are dominant in P^{NL}.

Comparison of equation (67B) to equation (46) yields the following expression for the third order nonlinear susceptibility at the Stokes frequency

$$\chi_s^{(3)} = \frac{N_0-N_1}{16\mu\omega_{01}} \left(\frac{\partial\alpha}{\partial q}\right)^2 \left[\frac{1}{\omega_{01} - \omega + i\Gamma}\right] \tag{69}$$

The susceptibility at other frequencies takes a similar form.

Energy Transfer Equations

The transfer of energy from the forward going pump pulse to the backward going Raman pulse is governed by Maxwell's wave equation

$$\frac{\partial^2 E}{\partial x^2} = \frac{n^2}{c^2}\left[\frac{\partial^2 E}{\partial t^2} + 4\pi\frac{\partial^2 P_{NL}}{\partial t^2}\right] \tag{70}$$

One dimensional analysis is sufficient for this treatment. If the amplitudes of the electric fields are assumed slowly varying

$$\frac{\partial^2 E_0}{\partial x^2} << K\frac{\partial E_0}{\partial x} \tag{71}$$

the second derivatives in equation (70) may be ignored. Substitution of the Stokes field, E_s, and the Stokes polarization P_s^{NL} from equations (63) and (67B) into equation (70) then yields

$$\frac{\partial|E_{s0}|^2}{\partial x} - \frac{n}{c}\frac{\partial|E_{s0}|^2}{\partial t} = \frac{-(N_0-N_1)}{2\mu\omega_{01}\Gamma}\left(\frac{\partial\alpha}{\partial q}\right)^2 \frac{\pi k_s \Gamma^2 |E_{p0}|^2 |E_{s0}|^2}{(\omega_{01}-\omega)^2+\Gamma^2} \tag{72}$$

Similarly, for the pump component one obtains

$$\frac{\partial|E_{p0}|^2}{\partial x} + \frac{n}{c}\frac{\partial|E_{p0}|^2}{\partial t} = \frac{-(N_0-N_1)}{2\mu\omega_{01}\Gamma}\left(\frac{\partial\alpha}{\partial q}\right)^2 \frac{\pi k_p \Gamma^2 |E_{p0}|^2 |E_{s0}|^2}{(\omega_{01}-\omega)^2+\Gamma^2} \tag{73}$$

In the above equations noting that $\omega_p^2 E >> \omega_p \frac{\partial E}{\partial t}$ has allowed the electric field amplitudes in the polarization to be treated as constants.

The above equations are readily expressed in terms of the intensity using the relationship

$$I = \frac{cn}{8\pi}|E|^2 \tag{74}$$

then

$$-\frac{\partial I_s}{\partial x} + \frac{n_s}{c}\frac{\partial I_s}{\partial t} = \gamma I_s I_p \tag{75}$$

$$\frac{\partial I_p}{\partial I_x} + \frac{n_p}{c}\frac{\partial I_p}{\partial t} = -\frac{\omega_p}{\omega_s}\gamma I_s I_p \tag{76}$$

where γ, the Stokes gain coefficient is given by

$$\gamma = \frac{4\pi^2 k_s (N_0 - N_1)}{\mu \omega_{01} \Gamma} \left(\frac{\partial \alpha}{\partial q}\right)^2 \frac{\Gamma^2}{(\omega_{01} - \omega)^2 + \Gamma^2} \qquad (77)$$

The expression for γ may be written in terms of the measurable Raman scattering cross section, $\frac{\partial \sigma}{\partial \Omega}$, using the relation

$$\frac{\partial \sigma}{\partial \Omega} = \left(\frac{2\mu\omega_0 c^4}{\omega^4 \hbar}\right)^{-1} \left(\frac{\partial \alpha}{\partial q}\right)^2 \qquad (78)$$

The expression for γ can be further simplified by assuming resonance, $\omega_{01} = \omega$, and by assuming $N_0 - N_1 = N$, the total population. These equations are valid for the conditions of the experiment.

The resulting expression is

$$\gamma = \frac{8\pi^2 c^2 N}{\hbar \omega_s^3 \Gamma} \left(\frac{\partial \sigma}{\partial \Omega}\right) \qquad (79)$$

Appendix II

This appendix describes the origins of the pulse delays observed in order to aid in pulse identification. The characteristic pulse separations observed in Chapter IV were the result of set transit times through the BSRS system as follows (see figure (13), page 35): 12 ns - the round trip time through the gas cell, 10 ns - the round trip time through the laser system starting from the dichroic mirror, and 2.5 or 5 ns - one or two round trips through the laser oscillator only. The table below summarizes the times at which pulse peaks were observed.

TIME(ns)		PULSES OBSERVED	DETECTOR
0	-	Pump pulse	Pump and REV
1	-	Depleted pump pulse	FWD
6	-	Pump pulse	FWD
12	-	Reverse Stokes pulse	REV
		Reverse Brillouin pulse	REV
22	-	Reamplified Brillouin pulse #1	Pump and REV
27	-	Reamplified Brillouin pulse #2	Pump and REV
28	-	Depleted reamp. Brill. pulse #1	FWD
		Forward Stokes pulse #1	FWD
33	-	Depleted reamp. Brill. pulse #2	FWD
		Forward Stokes pulse #2	FWD
34	-	2nd reverse Stokes pulse #1	REV
		2nd reverse Brillouin pulse #1	REV
39	-	2nd reverse Stokes pulse #2	REV
		2nd reverse Stokes pulse #2	REV

Appendix III

Three interesting plots of the output pulse shapes are displayed in figures 25, 26 and 27. The first two show the multipulse structure of the reverse Stokes pulse for two cases. The third depicts both the depleted pump pulse and the forward Stokes pulse, allowing a direct comparision.

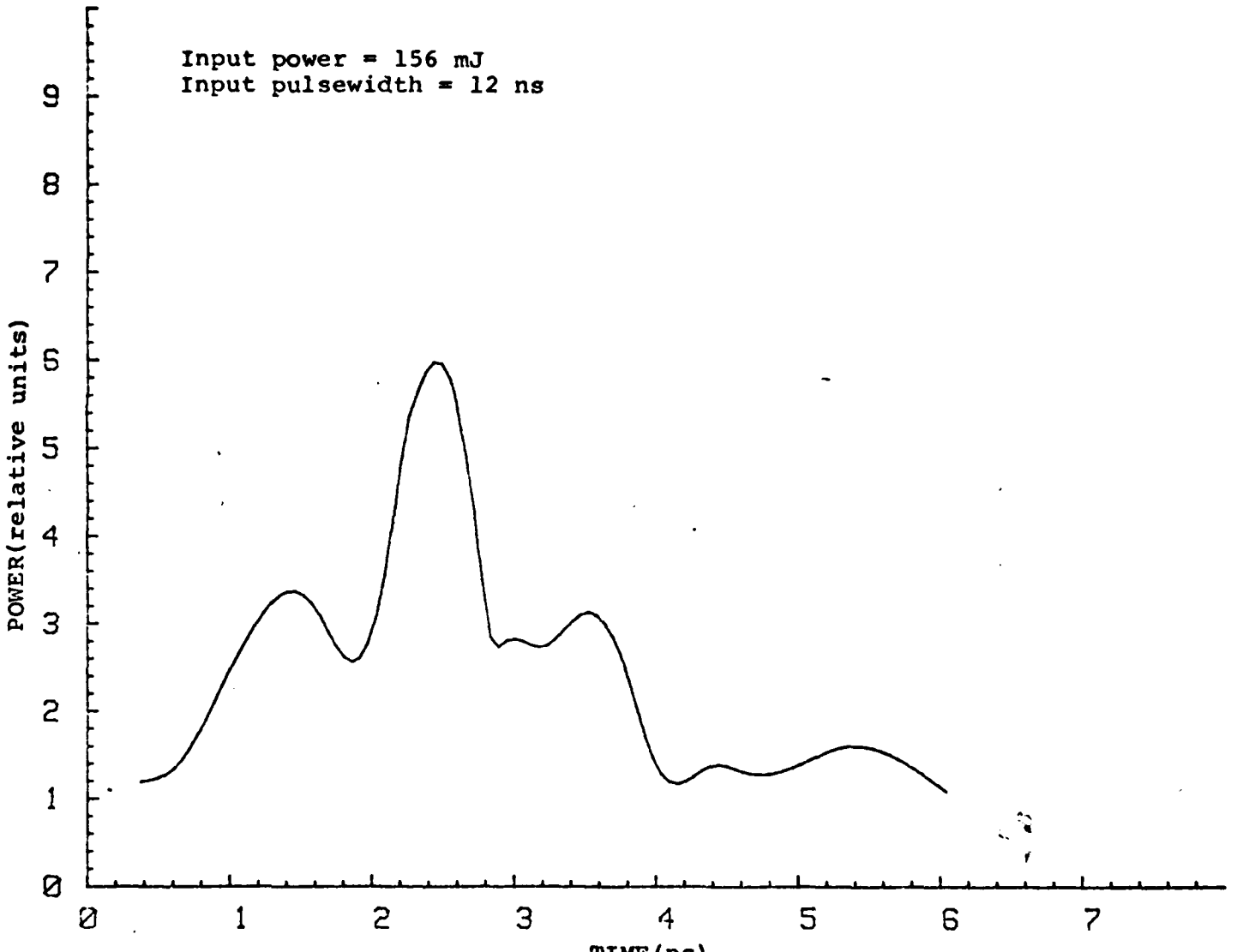

Fig. 25 Multipulse Reverse Stokes Output at 125 psi. Peak power is 2.3 MW.

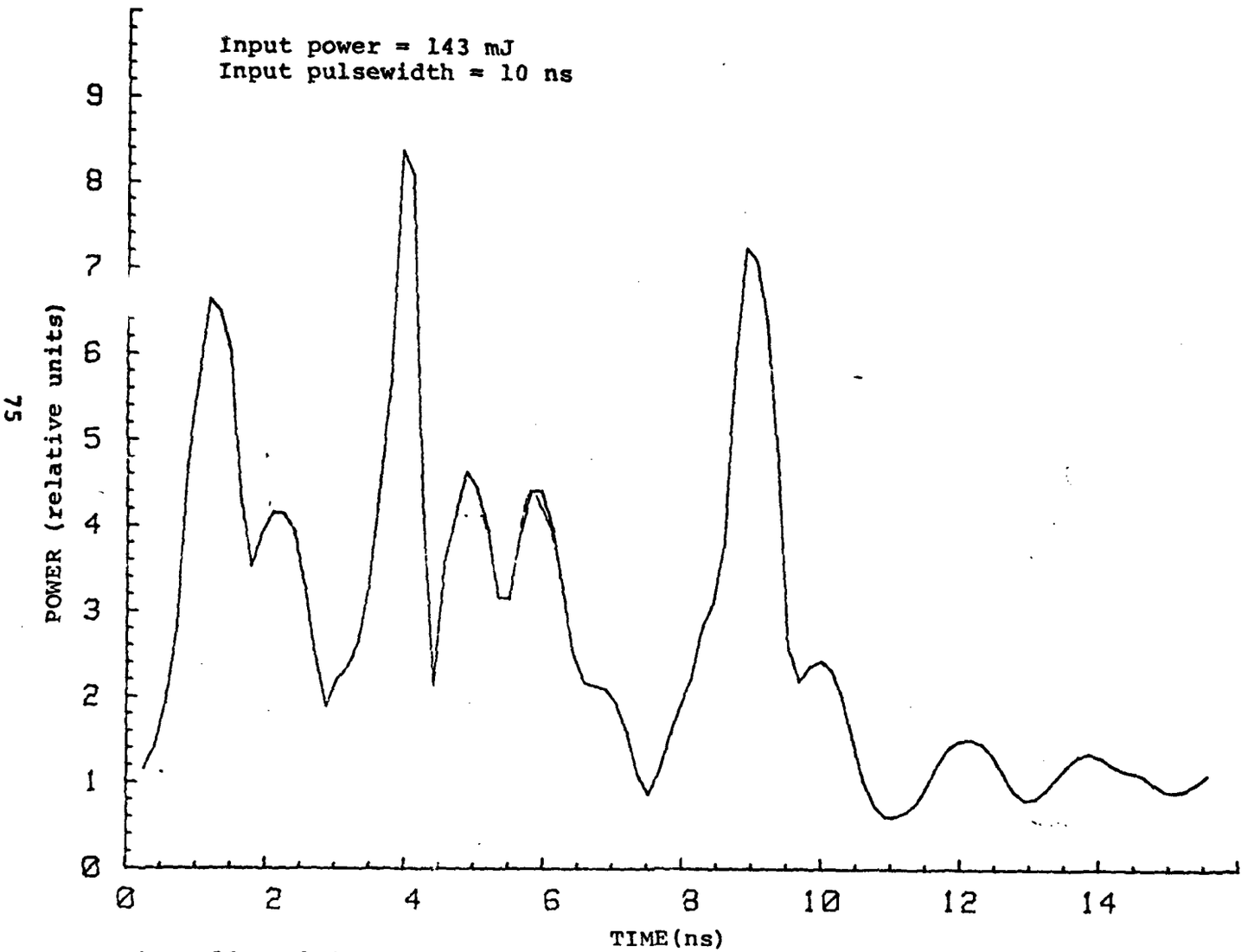

Fig. 26 Multipulse reverse Stokes output at 100 psi. Peak power is 4.7 KW.

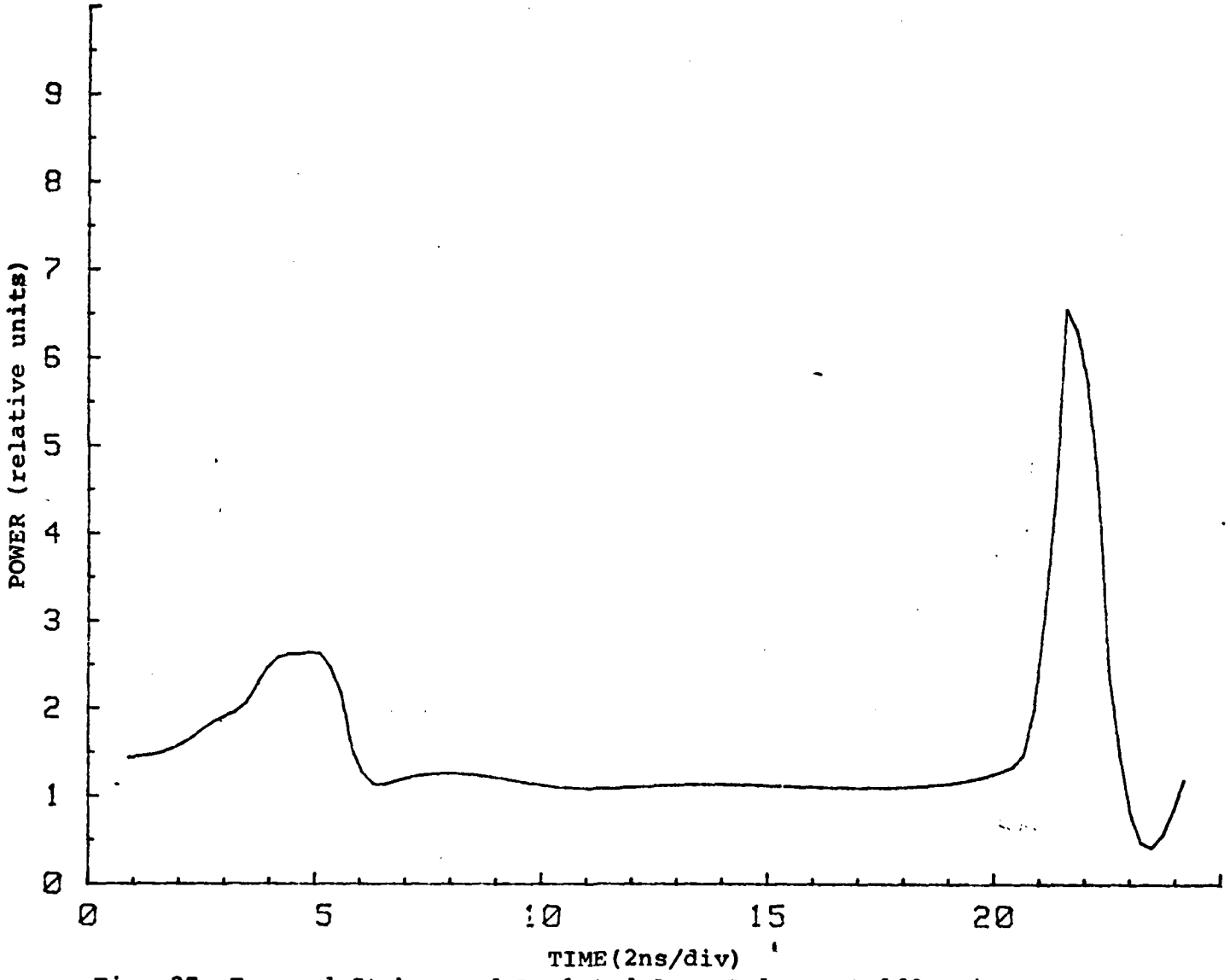

Fig. 27 Forward Stokes and Depleted Pump Pulses at 160 psi.

VITA

William D. Lindsay was born on 31 July 1958 in Cranston, Rhode Island. He graduated from Coventry High School in Coventry, Rhode Island in 1976 and attended Cornell University, Ithaca, New York from which he received the degree of Bachelor of Science in Electrical Engineering in May 1980. He was commissioned through AFROTC into the Air Force in May, 1980 and proceeded directly to active duty as a student at the School of Engineering, Air Force Institute of Technology in June, 1980.

UNCLASSIFIED

SECURITY CLASSIFICATION OF THIS PAGE (When Data Entered)

REPORT DOCUMENTATION PAGE	READ INSTRUCTIONS BEFORE COMPLETING FORM
1. REPORT NUMBER: AFIT/GEO/PH/81D-3	2. GOVT ACCESSION NO. AD-A113 173 / 3. RECIPIENT'S CATALOG NUMBER
4. TITLE (and Subtitle): DEVELOPEMENT OF A BACKWARD STIMULATED RAMAN SCATTERING SYSTEM FOR PULSE COMPRESSION	5. TYPE OF REPORT & PERIOD COVERED: MS Thesis
	6. PERFORMING ORG. REPORT NUMBER
7. AUTHOR(s): William D. Lindsay, 2nd Lt USAF	8. CONTRACT OR GRANT NUMBER(s)
9. PERFORMING ORGANIZATION NAME AND ADDRESS: (AFIT-EN) Air Force Institute of Technology, Wright-Patterson AFB, Ohio 45433	10. PROGRAM ELEMENT, PROJECT, TASK AREA & WORK UNIT NUMBERS
11. CONTROLLING OFFICE NAME AND ADDRESS	12. REPORT DATE: December 1981
	13. NUMBER OF PAGES: 86
14. MONITORING AGENCY NAME & ADDRESS(if different from Controlling Office)	15. SECURITY CLASS. (of this report): Unclassified
	15a. DECLASSIFICATION/DOWNGRADING SCHEDULE

16. DISTRIBUTION STATEMENT (of this Report)

Approved for public release; distribution unlimited

17. DISTRIBUTION STATEMENT (of the abstract entered in Block 20, if different from Report)

28 JAN 1982

18. SUPPLEMENTARY NOTES

FREDRIC C. LYNCH
Director, Public Affairs
Air Force Institute of Technology
Wright-Patterson AFB, Ohio

19. KEY WORDS (Continue on reverse side if necessary and identify by block number)

Raman Scattering
Backward Stimulated Raman Scattering
Methane
Picosecond Pulses

20. ABSTRACT (Continue on reverse side if necessary and identify by block number)

A Raman pulse compression system utilizing backward stimulated Raman scattering(BSRS) within a methane gas cell six feet in length was built and tested. A 12 MW giant pulse ruby laser with a pulsewidth of 12 ns(FWHM) was focused within the gas cell with a 10 cm focal length lens. The resulting reverse Stokes pulse at 8704 A had a maximum power of 15 MW and a minimum pulsewidth of 800 ps(FWHM). The peak power of the reverse Stokes

DD FORM 1 JAN 73 1473 EDITION OF 1 NOV 65 IS OBSOLETE

SECURITY CLASSIFICATION OF THIS PAGE (When Data Entered)

pulse as well as the threshold power for BSRS were measured as a function of pressure. The shortest and most intense reverse Stokes pulses were obtained in the pressure range of 150 -175 psi with an input energy of 125 - 160 mJ. The short, intense pulses produced by this system should be useful in the investigation of events occuring on a subnanosecond time scale such as semiconductor carrier diffusion processes. The competing nonlinear processes of stimulated Brillouin scattering (SBS) and gas breakdown were also investigated and found to limit the efficiency of this system to 10 percent.

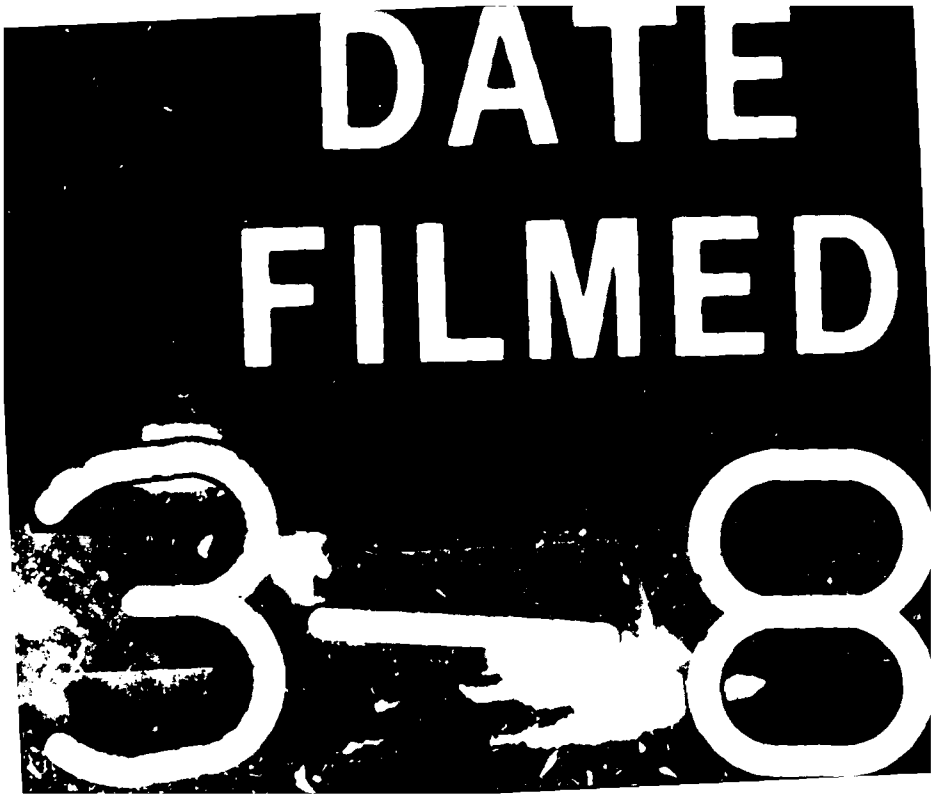
DATE
FILMED
8
8